Caveolar domain organization and trafficking is regulated by Abl kinases and mDia1

Asier Echarri[1,*], Olivia Muriel[1], Dácil M. Pavón[1], Hind Azegrouz[2], Fernando Escolar[3], María C. Terrón[3], Fátima Sanchez-Cabo[4], Fernando Martínez[4], María C. Montoya[2], Oscar Llorca[3] and Miguel A. del Pozo[1,*]

[1]Integrin Signaling Laboratory, [2]Cellomics Unit, Vascular Biology and Inflammation Department, and [4]Bioinformatics Unit, Centro Nacional de Investigaciones Cardiovasculares (CNIC), Melchor Fernández Almagro, 3, 28029, Madrid, Spain
[3]Centro de Investigaciones Biológicas, Consejo Superior de Investigaciones Científicas, Ramiro de Maeztu 9, 28040 Madrid, Spain
*Authors for correspondence (aecharri@cnic.es; madelpozo@cnic.es)

Journal of Cell Science 125, 4413

doi: 10.1242/jcs.120816

There was an error published in *J. Cell Sci.* **125**, 3097-3113.

The affiliations of the authors have been published incorrectly. The correct header of this article is shown above.

We apologise for this mistake.

Caveolar domain organization and trafficking is regulated by Abl kinases and mDia1

Asier Echarri[1,*], Olivia Muriel[1], Dácil M. Pavón[1], Hind Azegrouz[2], Fernando Escolar[3], María C. Terrón[3], Fátima Sanchez-Cabo[4], Fernando Martínez[4], María C. Montoya[2], Oscar Llorca[3] and Miguel A. del Pozo[1,*]

[1]Integrin Signaling Laboratory, Centro de Investigaciones Biológicas, Consejo Superior de Investigaciones Científicas, Ramiro de Maeztu 9, 28040 Madrid, Spain
[2]Cellomics Unit, Vascular Biology and Inflammation Department, Centro Nacional de Investigaciones Cardiovasculares (CNIC), Melchor Fernández Almagro 3, 28029 Madrid, Spain
[3]Centro de Investigaciones Biológicas, Consejo Superior de Investigaciones Científicas, Ramiro de Maeztu 9, 28040 Madrid, Spain
[4]Bioinformatics Unit, Centro Nacional de Investigaciones Cardiovasculares (CNIC), Melchor Fernández Almagro 3, 28029, Madrid, Spain
*Authors for correspondence (aecharri@cnic.es; madelpozo@cnic.es)

Accepted 4 March 2012
Journal of Cell Science 125, 3097–3113

doi: 10.1242/jcs.090134

Summary

The biology of caveolin-1 (Cav1)/caveolae is intimately linked to actin dynamics and adhesion receptors. Caveolar domains are organized in hierarchical levels of complexity from curved or flattened caveolae to large, higher-order caveolar rosettes. We report that stress fibers controlled by Abl kinases and mDia1 determine the level of caveolar domain organization, which conditions the subsequent inward trafficking of caveolar domains induced upon loss of cell adhesion from the extracellular matrix. Abl-deficient cells have fewer stress fibers, a smaller pool of stress-fiber co-aligned Cav1 and increased clustering of Cav1/caveolae at the cell surface. Defective caveolar linkage to stress fibers prevents the formation of big caveolar rosettes upon loss of cell adhesion, correlating with a lack of inward trafficking. Live imaging of stress fibers and Cav1 showed that the actin-linked Cav1 pool loses its spatial organization in the absence of actin polymerization and is dragged and clustered by depolymerizing filaments. We identified mDia1 as the actin polymerization regulator downstream of Abl kinases that controls the stress-fiber-linked Cav1 pool. mDia1 knockdown results in Cav1/caveolae clustering and defective inward trafficking upon loss of cell adhesion. By contrast, cell elongation imposed by the excess of stress fibers induced by active mDia1 flattens caveolae. Furthermore, active mDia1 rescues the actin co-aligned Cav1 pool and Cav1 inward trafficking upon loss of adhesion in Abl-deficient cells. Thus, caveolar domain organization and trafficking are tightly coupled to adhesive and stress fiber regulatory pathways.

Key words: Vesicle trafficking, Actin cytoskeleton, Cell adhesion, Abl tyrosine kinases, Caveolin-1

Introduction

Changes in cell adhesion to the extracellular matrix (ECM) induce changes in cell morphology through coordinated adjustments to the plasma membrane (PM) and the actin cytoskeleton (Parsons et al., 2010). The PM contains small domains characterized by the concentration of specific lipids and proteins. One such domain is defined by Cav1, a protein found in PM, focal adhesions, endomembranes, Golgi apparatus and cytosol (Hayer et al., 2010; Nethe et al., 2010; Parton and Simons, 2007; Pelkmans et al., 2004; Tagawa et al., 2005). Cav1 is required to form caveolae, a PM domain with the form of a Ω-shaped invagination (Parton and Simons, 2007). Cav1 is also found in other structures, such as rosettes decorated with caveolar domains, tubules and non-caveolar PM domains (flattened caveolae) (Bundgaard et al., 1983; Hill et al., 2008; Parton et al., 1994; Peters et al., 2003; Sinha et al., 2011; Verma et al., 2010). The pathways regulating caveolar domains are largely unknown. Recently, the cavin family, pacsin2 and EHD2 have been shown to regulate caveolae biology (Aboulaich et al., 2004; Hansen et al., 2011; Hansen and Nichols, 2010; Hill et al., 2008; Moren et al., 2012; Senju et al., 2011; Stoeber et al., 2012). Cav1 is an important regulator of multiple signaling pathways, cell mechanosensing ability and lipid biology (Parton and Simons, 2007; Pol et al., 2001; Rizzo et al., 1998; Yu et al., 2006).

Although no specific cargo for caveolae has been unambiguously identified, there is much accumulated information on caveolae trafficking and Cav1 dynamics. Studies using fluorescence techniques indicate that adherent cells contain a pool of relatively static Cav1 (Mundy et al., 2002; Thomsen et al., 2002). However, certain cell types contain a distinct pool of highly mobile Cav1 vesicles (Mundy et al., 2002; Pelkmans and Zerial, 2005). Caveolae endocytosis can be triggered by several stimuli, including changes in lipid composition (Le Lay et al., 2006; Sharma et al., 2004), viral infection (Pelkmans et al., 2001), phosphatase inhibition and hyperosmotic stress (Parton et al., 1994), and loss of integrin-mediated cell adhesion (del Pozo et al., 2005). Upon loss of cell adhesion, Cav1-positive PM domains labeled for various membrane raft markers, including GM1, initiate an inward traffic to the perinuclear area (Balasubramanian et al., 2007; del Pozo et al., 2004; Gaus et al., 2006). This plasma membrane remodeling, characterized by the formation of large caveolar rosettes and mediated by Cav1, regulates Rac1 PM targeting (del Pozo et al., 2005; Goetz et al., 2011). Cav1 is important for directional cell migration, where local loss of adhesion is essential (Grande-García

Journal of Cell Science

et al., 2007), and for the regulation of anchorage independent growth, a key feature of cancer cells (Cerezo et al., 2009; Schwartz, 1997; Williams and Lisanti, 2005). Both these processes involve an essential regulatory role of Cav1-directed Rac1 PM targeting. Loss of cell-adhesion-induced apoptotic signals must be overcome by metastatic cells entering the vasculature. Therefore, understanding the signaling pathways orchestrating adhesion regulated Cav1 trafficking is important for defining the role of Cav1 in anchorage independent growth.

Several studies suggest that Cav1 and caveolae are tightly associated with the actin cytoskeleton (Kanzaki and Pessin, 2002; Morone et al., 2006; Richter et al., 2008; Stahlhut and van Deurs, 2000). Electron microscopy identified a pool of caveolae decorating stress fibers, and Cav1 frequently co-aligns with

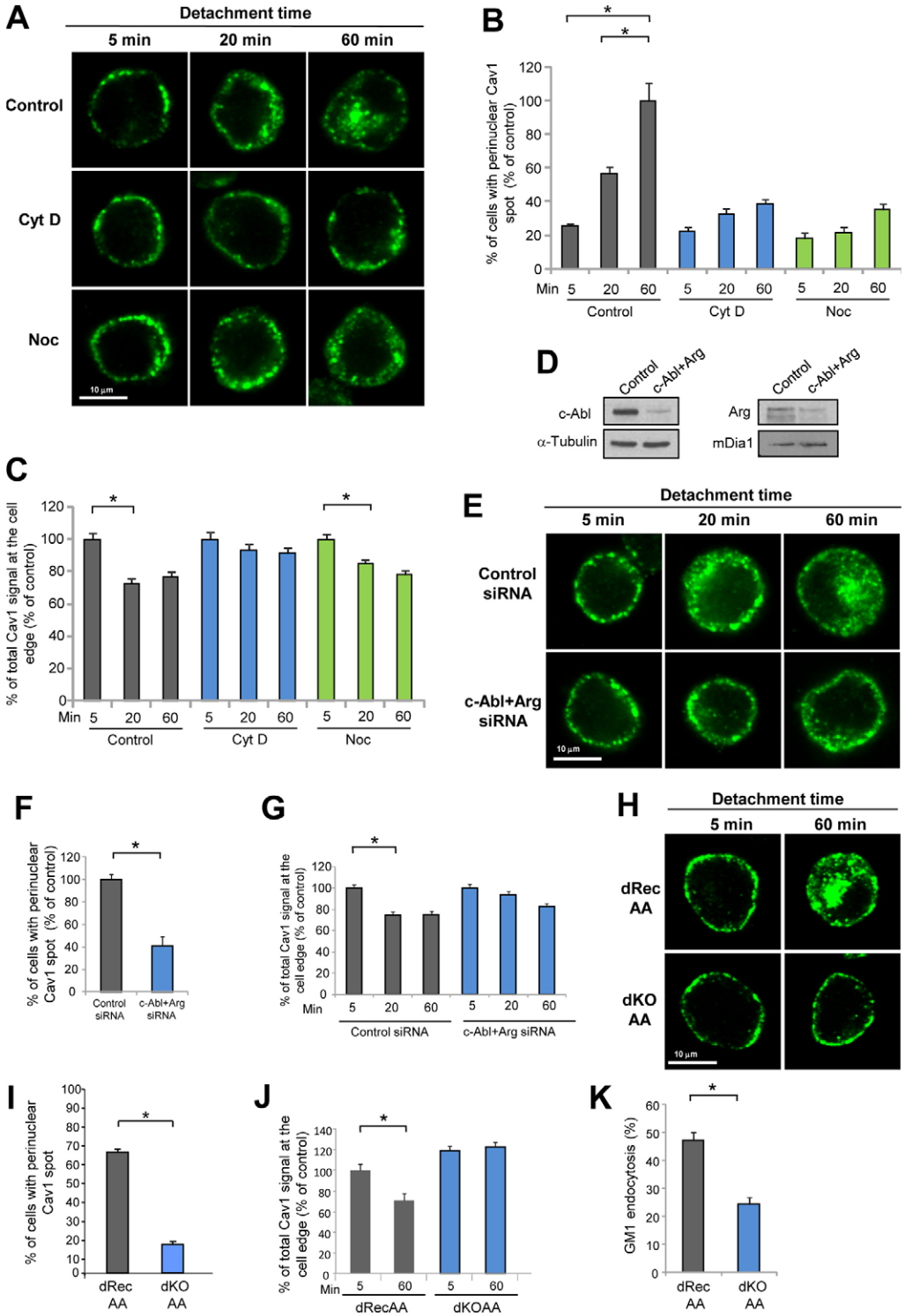

Fig. 1. See next page for legend.

actin fibers in immunofluorescence studies (Rothberg et al., 1992; Stahlhut and van Deurs, 2000). However, although actin clearly plays a role in Cav1 biology, the mechanism and upstream pathways through which actin polymerization regulates adhesion-regulated Cav1/caveolae organization and trafficking are poorly understood.

Actin polymerization is a complex process regulated by multiple pathways. Linear actin cables are polymerized by the action of formins, including mDia1, which regulates actin stress fibers and microtubules downstream of RhoA (Palazzo et al., 2001; Watanabe et al., 1999). Branched actin polymerization is induced by the Arp2/3 complex, which acts downstream of Rac and Cdc42 (Goley and Welch, 2006; Higgs and Pollard, 2001). This type of actin polymerization is important in the formation of lamellae and actin tails and in clathrin-mediated endocytosis (Chhabra and Higgs, 2007).

Two key regulators of the actin cytoskeleton are the Abl tyrosine kinases c-Abl and Arg (Hernández et al., 2004; Woodring et al., 2003). c-Abl phosphorylates Cav1 (Sanguinetti and Mastick, 2003) and numerous substrates involved in actin cytoskeleton regulation (Bradley and Koleske, 2009). In *Drosophila*, lack of dAbl induces mislocalization of Arp2/3 and of the formin family member diaphanous (*Drosophila* homolog of mDia), suggesting that Abl tyrosine kinases regulate both types of actin nucleator (Grevengoed et al., 2003). Abl tyrosine kinases are also involved in EGFR trafficking, cell entry by several pathogens, and other actin-dependent processes (Bradley et al., 2006; Burton et al., 2003; Reeves et al., 2005; Smith-Pearson et al., 2010; Tanos and Pendergast, 2006; Woodring et al., 2002).

Here we show that sudden loss of cell adhesion induces the formation of large caveolar rosettes that form before the accumulation of Cav1 in the perinuclear area. This process is dependent on Abl tyrosine kinases. Mechanistically, Abl regulates the actin fiber co-aligned Cav1 pool and determines its correct spatial organization around actin, needed to arrange caveolar domains into large rosettes upon loss of cell adhesion. We identify mDia1 as the actin regulator downstream of Abl kinases that controls caveolae organization and trafficking. Notably, active mDia1 induces an excess of stress fibers in adherent cells that flattens caveolae, an effect opposite to the caveolae clustering observed upon silencing of mDia1 or Abl. Thus caveolar domain plasticity, organized in shapes ranging from flattened caveolae to caveolar rosettes, is tightly coupled to adhesive and stress fiber regulatory pathways.

Fig. 1. Actin, microtubules and Abl tyrosine kinases regulate Cav1 inward trafficking. (**A**) Cytochalasin D (Cyt D) and nocodazole (Noc) block endogenous Cav1 inward trafficking. HeLa cells were detached, fixed at the indicated times and confocal images taken at the cell equator. DMSO, Cyt D or nocodazole were added 5 minutes before detachment and maintained during suspension. (**B**) Quantification of the internal endogenous Cav1 pool in detached cells as in A. Cells showing perinuclear accumulation of Cav1 were blind-scored as positive, and the number of control cells showing this accumulation 60 minutes after detachment was set at 100%. $n=3$. (**C**) Quantification of the cell-edge endogenous Cav1 pool in cells as in A. The amount of Cav1 at the cell edge was normalized to the total amount of Cav1 in each cell. Data are normalized to control cells 5 minutes after detachment. Note that cell-edge Cav1 was not significantly reduced after 20 minutes in Cyt-D-treated cells. $n=36$–111. (**D**) Immunoblot showing specific suppression of c-Abl and Arg expression in HeLa cells transfected with c-Abl+Arg siRNAs. Loading controls are shown in the lower blots. (**E**) Knockdown of c-Abl and Arg blocks endogenous Cav1 inward trafficking. HeLa cells transfected with control or c-Abl+Arg siRNAs were placed in suspension, fixed and stained at the indicated times. Images show representative confocal sections taken at the cell equator. (**F**) Quantification of spot-like localization of endogenous Cav1 in the perinuclear area 60 minutes after detachment of HeLa cells transfected with c-Abl+Arg siRNAs. $n=3$. (**G**) Quantification of the cell-edge endogenous Cav1 pool in cells treated as in E. The amount of Cav1 at the cell edge was normalized to the total amount of Cav1 in each cell. Data are normalized to control cells 5 minutes after detachment. Note that cell-edge Cav1 is not significantly reduced after 20 minutes in cells transfected with c-Abl+Arg siRNAs. $n=39$–90. (**H**) Representative confocal images showing endogenous Cav1 distribution in detached dRecAA and dKOAA MEFs. Confocal images show transfer of Cav1 to the cell interior in dRecAA cells but retention at the cell periphery in dKOAA cells. (**I**) Quantification of spot-like localization of endogenous Cav1 in the perinuclear area of dRecAA and dKOAA cells 60 minutes after detachment. $n=3$. (**J**) Quantification of the cell-edge endogenous Cav1 pool in cells treated as in H. The amount of Cav1 at the cell edge was normalized to the total amount of Cav1 in each cell. Data are normalized to control cells 5 minutes after detachment. (**K**) Endocytosis of GM1 is reduced in dKOAA cells. Cells were kept in suspension for 0.25 or 120 min. Cells were then placed at 4℃ and cell-surface-bound CTB–Alexa-Fluor-647–GM1 complex was quantified by FACS. Endocytosis was calculated as the percentage drop in surface GM1 levels after 120 minutes in suspension. $n=6$.

Results

Abl tyrosine kinases regulate Cav1 inward trafficking

Apart from the roles of dynamin2 and phospho-Cav1, little is known about the pathways regulating the trafficking of Cav1 from the cell edge to the perinuclear area upon loss of cell adhesion (del Pozo et al., 2005). To investigate the involvement of cytoskeletal filaments in this process, we disrupted the actin and microtubular cytoskeletons in HeLa cells and measured the trafficking of endogenous Cav1. Within 20 minutes of non-adherent culture, a fraction of Cav1 moved from the cell edge and started to traffic to the perinuclear area, where by 60 minutes it accumulated in a clustered spot (hereafter perinuclear Cav1 spot; Fig. 1A), similar to observations in fibroblasts (del Pozo et al., 2005). The percentage of cells with the perinuclear Cav1 spot increased with time in suspension (from 5 to 60 minutes; Fig. 1A,B). Disruption of the actin cytoskeleton (with cytochalasin D; Cyt D) or microtubules (nocodazole) reduced the number of cells with the perinuclear spot at 60 minutes by ~60% (Fig. 1A,B). Accumulation of Cav1 in the perinuclear spot was accompanied by a reduction in the pool of Cav1 at the cell edge (Fig. 1A). The Cav1 pool at the cell edge was quantified in cells stained with the PM marker wheat-germ-agglutinin–Rhodamine, using specialized software (supplementary material Fig. S1A). In control cells, the cell-edge Cav1 pool was reduced by ~28% after 20 minutes, similar to the levels detected after 60 minutes (Fig. 1A,C). Cyt D completely prevented the movement of Cav1 from the cell edge during the first 20 minutes (Fig. 1A,C). Over longer periods in suspension (60 min), the signal remained at the cell periphery (Fig. 1A,C). Nocodazole did not prevent Cav1 from leaving the cell edge and this Cav1 pool trafficked out of the cell edge (Fig. 1A,C). However nocodazole prevented the formation of the perinuclear Cav1 spot and distributed Cav1 throughout the cytosol (Fig. 1A,B). Similar results were obtained using HeLa cells expressing low levels of Cav1–GFP (supplementary material Fig. S1B–D). These results are consistent with previous studies on GM1 and Cav1 trafficking (Balasubramanian et al., 2007; Mundy et al., 2002; Parton et al., 1994) and suggest that Cav1 inward trafficking upon loss of cell adhesion requires actin polymerization

in the initial stages and microtubules in the later stages prior to accumulation in the perinuclear area.

To investigate the pathways regulating Cav1 inward trafficking, we focused on Abl tyrosine kinases, known regulators of the actin cytoskeleton (Bradley and Koleske, 2009) and Cav1 phosphorylation (Sanguinetti and Mastick, 2003). siRNAs for c-Abl and Arg effectively silenced both proteins (Fig. 1D) and reduced the trafficking of endogenous Cav1 and Cav1–GFP to the perinuclear spot by ~60% (Fig. 1E,F; supplementary material Fig. S1E–G); this inhibition was similar to that induced by dynamin2 silencing (supplementary material Fig. S1G). Perinuclear Cav1 accumulation was similarly inhibited by a different set of siRNAs for both tyrosine kinases (control 100±6.5; c-Abl+Arg 50.2±2.4, $P=0.0007$). Independent knockdown of c-Abl and Arg showed that most of the effect was due to c-Abl, but that Arg also contributed (supplementary material Fig. S1I). We therefore knocked down both proteins throughout the study. In cells expressing control siRNA, the cell-edge endogenous Cav1 pool was reduced by ~25% after 20 minutes in suspension and accumulated in the cytosol (Fig. 1E,G); in contrast, Abl+Arg siRNA had little effect on the removal of Cav1 from the cell edge at 20 minutes but slightly inhibited it by 60 minutes (25% reduction in control and 17% in c-Abl+Arg knockdown cells) (Fig. 1E,G). Similar results were obtained with Cav1–GFP (supplementary material Fig. S1F,H). This indicates that Abl tyrosine kinases regulate the early stages of Cav1 inward trafficking, and that their depletion slows this process. To confirm these observations, we examined endogenous Cav1 trafficking in MEFs deficient for c-Abl and Arg (dKOAA) and in dKOAA MEFs reconstituted with c-Abl and Arg (dRecAA) (supplementary material Fig. S1J) (Plattner et al., 2003). Cell detachment of dRecAA cells induced efficient trafficking of Cav1 to the perinuclear area and formation of the perinuclear spot, but this was impaired by ~77% in dKOAA cells (Fig. 1H,I). Notably, the cell-edge Cav1 pool was fully retained at the cell edge in the absence of Abl kinases (Fig. 1H,J). These results prompted us to test whether Abl kinases regulate the endocytosis of cholera toxin B subunit (CTB) ligand GM1. Cells lacking Abl kinases showed a 50% reduction in the endocytosis of GM1 (Fig. 1K). Thus, Abl kinases are, like the actin cytoskeleton, required for the initiation of Cav1 inward trafficking from the cell edge.

Abl kinases spatially organize caveolar domains and regulate the actin co-aligned Cav1 pool

We noticed that some of the Cav1-positive vesicle-like spots at or close to the PM appeared to be brighter in cells transfected with c-Abl+Arg siRNAs or treated with Cyt D. We quantified in an automated manner the brightness of endogenous Cav1 spots using total internal reflection fluorescence (TIRF) microscopy (TIRF-m; see Materials and Methods; supplementary material Fig. S2A) in dRecAA and dKOAA cells. Analysis of over 40,000 Cav1 spots showed a shift in the distribution of the intensity of the vesicles towards brighter spots in dKOAA cells compared to control cells (Fig. 2A,B). The shift was evident both for the overall distributions (dRecAA median=20.2 vs dKOAA median=24.33, $P<10^{-4}$) but also for the proportion of Cav1 spots with high intensity or q4 population (25% dRecAA vs 31.3% dKOAA, $P<10^{-4}$; Fig. 2C). High intensity vesicles were defined as those with a signal over the 75% percentile of the distribution of intensities in the control cells (q4 bars in Fig. 2C). Dim spots, represented in the q1 population, were lower in dKOAA cells, which might indicate a contribution of dim spots to the formation of bright spots (Fig. 2C). Similar results were obtained by silencing c-Abl+Arg, which revealed that bright endogenous Cav1 spots were 13% more abundant in the q4 population (supplementary material Fig. S2B,C). A similar effect was observed when this analysis was performed in cells expressing Cav1–GFP as the readout (supplementary material Fig. S2D). These results suggest that Cav1 vesicles undergo some clustering process in the absence of Abl kinases. To understand more precisely the nature of endogenous Cav1 clustering, we examined HeLa cells silenced for both kinases by electron microscopy (EM). We scored morphologically recognizable caveolae at the plasma membrane and caveolar domains in rosettes (or rosette-caveolae). We then measured the distance between adjacent caveolar domains to detect clustering. This analysis showed that Abl kinases silencing significantly increased the numbers of caveolae and rosette-caveolae that were close to each other (less than 300 nm apart; Fig. 2D,F). This difference was due to an increase in rosette-caveolae and the closer proximity of caveolae (Fig. 2F). These observations were more evident in MEFs deficient for Abl kinases that showed an increase in caveolae, rosette-caveolae and clustered caveolar domains, compared to control cells (Fig. 2E,G). Notably, isolated caveolae (more than 300 nm apart) did not show a significant increase in Abl deficient MEFs (Fig. 2G) or HeLa cells silenced for both kinases (Fig. 2F). The size of caveolar rosettes and the density of rosette-caveolae within rosettes were similar in dRecAA or dKOAA cells in attached conditions (Fig. 2G). Although the immunofluorescence and EM images may not measure the same minimum caveolar structures due to resolution limitations in immunofluorescence images, these results are consistent with the increase in Cav1 spot brightness observed by immunofluorescence in cells lacking (or silenced for) Abl kinases, and are similar to those observed by EM upon Cyt D treatment (Fujimoto et al., 1995). We next analyzed the caveolar domains formed upon detachment from the ECM by EM. In control MEFs, the number of rosettes was increased 8 fold, which led to a similar increase in rosette-caveolae, but non-rosette-associated caveolae remained constant (Fig. 2E,G). Interestingly, the size of these rosettes differed significantly from the few observed in attached cells. Upon loss of cell adhesion, the rosette area increased 3 fold (Fig. 2E,G). EM analysis of ruthenium red-stained detached cells indicated that virtually all the rosettes (94.0±3.9%) were still surface connected (supplementary material Fig. S2K), as previously reported in adherent cells (Bundgaard et al., 1983; Parton et al., 1997). Caveolar rosette density was reduced by 60 minutes in non-adherent conditions (from 4.0±1.5/100 μm at 5 minutes to 0.6±0.2/100 μm at 60 minutes; $P=0.03$; supplementary material Fig. S2K). This coincides with trafficking of Cav1 to the perinuclear area, as detected by immunofluorescence (Fig. 1H), where it colocalizes with recycling endosome markers such as Rab11 (Muriel et al., 2011). This could be explained by a mechanism in which rosette-caveolae are pinched off from rosettes, or by a flattening of rosette-caveolae as rosettes traffic to the perinuclear area, preventing their identification by morphological criteria; the latter possibility is also consistent with a pinch-off of the whole rosette structure. Caveolar domains respond to tension (Kozera et al., 2009; Sinha et al., 2011), and the increase in caveolar domain complexity observed in suspended cells might therefore reflect an adaptation to sudden loss of membrane tension,

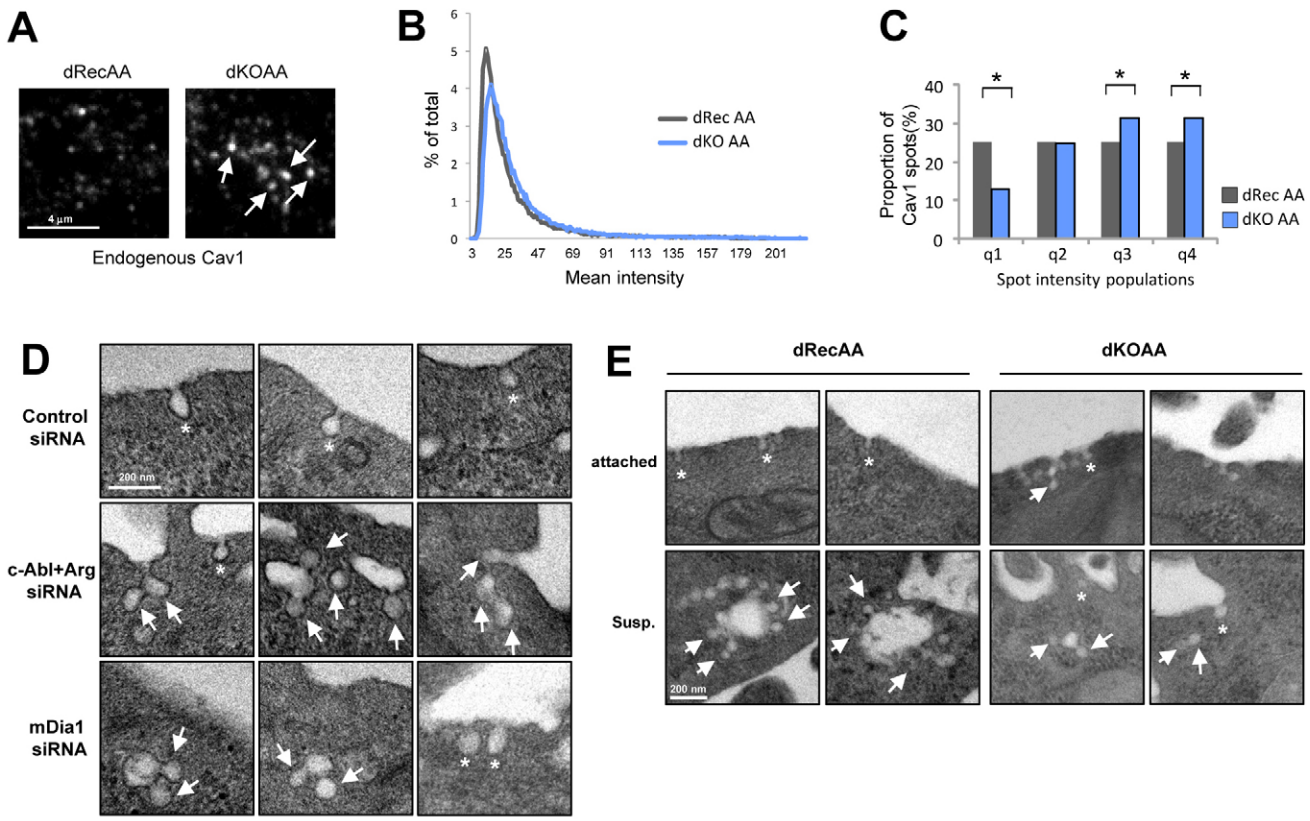

F

siRNA	Number of Caveolae /100 μm	Number of Rosette-caveolae /100 μm	Caveolae+rosette-caveolae /100 μm	Rosettes ≥2 rosette-caveolae /100 μm	Number of clustered caveolae + clustered rosette-caveolae/100 μm	Number of isolated caveolae + isolated rosette-caveolae/100 μm
Control	4.65±0.9	3.40±1.01	8.05±1.46	1.02±0.3	3.26±1.1	4.66±0.7
c-Abl+Arg	3.00±0.8 (p=0.18)	**9.65±2.35** (p=0.021)	12.65±2.55 (p=0.18)	**4.05±0.9** (p=0.006)	**9.63±2.2** (p=0.017)	3.02±0.8 (p=0.14)
mDia1	5.9±1.5 (p=0.48)	7.01±1.92 (p=0.10)	12.72±2.46 (p=0.18)	2.56±0.7 (p=0.08)	**7.98±1.6** (p=0.027)	4.74±1.3 (p=0.96)

G

Cell line	Number of Caveolae /100 μm	Number of Rosette-caveolae /100 μm	Caveolae+rosette-caveolae /100 μm	Rosettes ≥2 rosette-caveolae /100 μm	Number of clustered caveolae + clustered rosette-caveolae/100 μm	Number of isolated caveolae + isolated rosette-caveolae/100 μm	Area rosette (μm²)	Rosette-caveolae/100 μm of rosette
dRec AA attached	3.32±0.6	1.3±0.4	4.82±0.8	0.53±0.1	2.18±0.6	2.64±0.5	32.2±11.0	317±52
dKO AA attached	**7.80±1.4 (p=0.007)**	**4.12±1.0 (p=0.019)**	**12.76± (p=0.002)**	**1.65±0.4 (p=0.017)**	**9.13±1.8 (p=0.0008)**	3.63±1.3 (p=0.36)	33.4±9.2	366±28
dRec AA suspension	5.37±1.2	13.4±4.7 (p=0.01)	19.0±5.0 (p=0.01)	4.02±1.3 (p=0.016)	12.05±4.3 (p=0.03)	7.02±1.6 (p=0.01)	95.8±14.2 (p=0.001)	184±20(p=0.03)
dKO AA suspension	3.65±0.9 (p=0.02)	3.68±1.3 (p=0.056)	**7.17±1.6 (p=0.03)**	1.38±0.5	4.0±1.4(p=0.03)	**3.1±0.7 (p=0.04)**	68.8±20.4	256±38 (P=0.02)

Fig. 2. Abl kinases organize endogenous Cav1 and caveolar domains. (**A**) Absence of Abl kinases induces formation of bright endogenous Cav1 spots. Representative TIRF-m images of endogenous Cav1 spots. Arrows marked bright Cav1 clusters. (**B**) Analysis of the spot intensity distribution of endogenous Cav1 in dRecAA and dKOAA cells. The relative frequency of each intensity value in the whole population is represented. 40,387 (dRecAA) and 46,253 spots (dKOAA) were analyzed. (**C**) There are more bright endogenous Cav1 spots in Abl-deficient cells. The Cav1 spot intensity values separated into four populations (q1 being the dimmest spots and q4 the brightest spots), as indicated in the Materials and Methods, are shown for both cell lines. *χ^2-test $P<10^{-5}$. (**D**) Abl kinases and mDia1 regulate caveolar domain organization. HeLa cells treated with the indicated siRNA were analyzed by EM and representative images are shown. Isolated caveolae and rosette-caveolae are marked with asterisks and arrows, respectively. (**E**) Representative EM images of dRecAA and dKOAA cells. Isolated caveolae and rosette-caveolae are marked with asterisks and arrows, respectively. Contrast and brightness were modified individually. (**F**,**G**) Abl kinases and mDia1 regulate caveolar domain organization. Quantification of caveolar domain structures analyzed by EM in the different cell lines or treatments is shown. Student's two-tailed *t*-test *P*-values are shown in brackets and in bold if below 0.05 compared with the corresponding control. *P*-values highlighted in grey compare the same cell line under attached or suspended (susp.) conditions; $n=17–41$. A minimum of 765.6 and maximum of 1802.3 μm were analyzed.

reportedly occurring in such conditions (Colbert et al., 2009). In contrast, these increments in caveolar complexity parameters (number of rosettes, rosette-caveolae and rosette size) observed in dRecAA cells upon loss of cell adhesion were not observed in dKOAA cells (Fig. 2E,G). Together, these results show that upon loss of cell adhesion/tension, cells form large caveolar rosettes in an Abl-kinase-dependent manner. The fact that absence of Cav1 inward trafficking in Abl-deficient suspended cells correlates with clustering of caveolae in Abl-deficient attached cells suggests that this atypical distribution in attached cells may prevent the formation of large rosettes observed upon loss of cell adhesion. Abl kinases are activated in response to cell adhesion but not to detachment (Lewis et al., 1996), arguing against an active role once the cells are detached; instead their role would be to organize an actin-linked Cav1 pool in attached cells.

Since actin or Abl kinases depletion showed similar phenotypes, we asked whether the observed phenotypes were the result of Abl kinase-mediated regulation of the alignment of Cav1 with actin fibers (Stahlhut and van Deurs, 2000). The pool of actin co-aligned Cav1 was reduced twofold in c-Abl+Arg deficient cells compared with control cells (Fig. 3A,B). To investigate the cause(s) of this difference, we analyzed F-actin distribution and measured the amount of stress fibers in both cell lines. The analysis of F-actin distribution in the different areas of

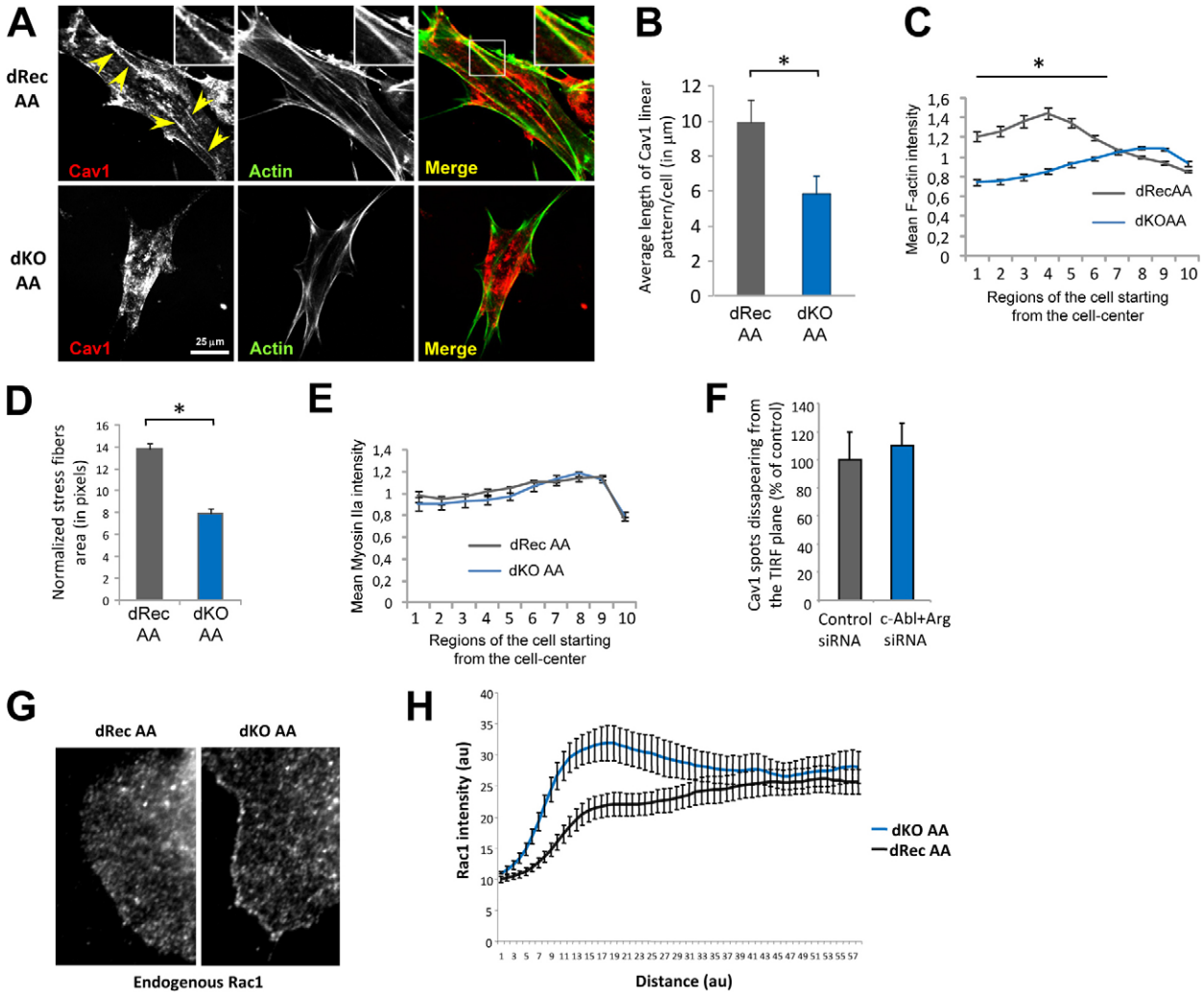

Fig. 3. Abl kinases regulate stress fibers, an actin fiber co-aligned Cav1 pool but do not control Cav1 z-movement. (**A**) The linear distribution of Cav1 is disrupted in the absence of Abl kinases. dRecAA and dKOAA MEFs were plated on fibronectin-coated surfaces and stained for Cav1 (red) and actin (pseudocolored in green) and examined by confocal microscopy. Arrowheads indicate linear Cav1 distribution. (**B**) Quantification of linear Cav1. The length of each Cav1 line was measured blind and the total length was summed for each cell. $n=46$ and 51. (**C**) F-actin distribution is disrupted in the absence of Abl kinases. F-actin average intensity was measured in concentrically drawn imaginary circles starting from the center of the cell (numbered 1 in the graph). $n=63$ and 81. (**D**) Stress fibers are reduced in Abl deficient cells. Stress fiber area normalized to the total analyzed area in each cell is represented. $n=83$ and 79. (**E**) Myosin IIa distribution is not regulated by Abl kinases. Myosin IIa average intensity was measured in 10 concentrically drawn imaginary circles starting from the center of the cell (as in C). $n=45$ and 20. (**F**) Cav1 z-movement is not regulated by Abl tyrosine kinases. Disappearance of Cav1–GFP spots from the TIRF plane was measured in control and c-Abl+Arg-silenced HeLa cells. (**G**) Plasma membrane targeting of endogenous Rac1 is regulated by Abl tyrosine kinases. Immunofluorescence of endogenous Rac1 in dRecAA and dKOAA cells allowed to spread on fibronectin (10 µg/ml) for 40 minutes. (**H**) Quantification of average Rac1 staining intensity in each pixel from the cell exterior to the cytoplasm. Twenty randomly selected cells of each cell type were analyzed. Intensity measurements were taken from 10 points on the cell edge and a line was drawn to the cell interior. Mean intensity values ± s.e.m. are shown at each position (in pixels). au, arbitrary units.

the cell indicated that in the central area of the cells (rings 1–6) the relative F-actin intensity was significantly decreased in dKOAA cells (Fig. 3C), despite the fact that the average F-actin intensity in the whole cell was slightly higher in dKOAA cells (0.13 ± 0.004 vs 0.17 ± 0.007, $P<0.001$). This rules out a global defect on F-actin in Abl-deficient cells and suggests that a deficiency in stress fibers in the center of the cell might cause these differences. In order to determine the essence of these differences, a quantification of areas of fibrillar actin was carried out using Definiens software as described in the Materials and Methods. A normalized quantitative value representing stress fiber organization was calculated for both cell lines. This analysis showed that dKOAA cells have significantly reduced stress fibers (Fig. 3D). We also quantified the amount and distribution of myosin IIa. While average myosin IIa staining was slightly higher in dKOAA cells (0.17 ± 0.004 in dRecAA vs 0.23 ± 0.01 in dKOAA) the distribution in the cell was similar in both cell lines and no gross defects were observed in the stained structures (Fig. 3E, and data not shown). Thus, Abl kinases regulate the amount of stress fibers, the Cav1 pool co-aligned with stress fibers, caveolar domain organization, and inward trafficking.

During cell detachment there is a drop in plasma membrane tension (Colbert et al., 2009) and Cav1 leaves the plasma membrane. This inward movement is dependent on actin and Abl kinases. In order to understand the specificity of Abl regulation on Cav1 dynamics we analyzed another type of Cav1 movement. A freely moving Cav1 pool has been shown to move rapidly in and out the TIRF plane in attached cells (hereafter z-movement) (Pelkmans and Zerial, 2005). This movement, also named kiss-and-run, was not affected by silencing of Abl kinases or dynamin2 (with two independent siRNAs; Fig. 3F and supplementary material Fig. S2G,H), suggesting that Cav1 z-movement and Cav1 inward trafficking are independently regulated.

Since Cav1 inward trafficking regulates both directional migration and anchorage independent growth through Rac1 PM targeting (Cerezo et al., 2009; Goetz et al., 2011; Grande-García et al., 2007), we monitored Rac1 at the leading edge of Abl-deficient spreading cells. Rac1 at the leading edge of spreading fibroblasts was increased in MEFs deficient for Abl kinases (Fig. 3G,H).

Actin spatially organizes a pool of Cav1 spots

The clusters of endogenous Cav1 observed upon silencing of Abl kinases resembled those formed upon Cyt D treatment (Fujimoto et al., 1995; Thomsen et al., 2002), prompting us to compare the effect of Abl kinase silencing and actin disruption on Cav1 spot distribution. In cells treated with Cyt D, endogenous Cav1 was clustered and the proportion of bright Cav1 spots in the q4 was ~35% higher than in untreated cells (Fig. 4A,B). To further investigate the effect of actin disruption on Cav1 clustering we used Cav1–GFP and the actin probe lifeact. We first confirmed that Cyt D treatment under our conditions induced Cav1–GFP clustering, as previously observed (Thomsen et al., 2002). Mis-targeting of Cav1–GFP has been reported (Hayer et al., 2010), and therefore conclusions obtained with Cav1–GFP must be validated with endogenous Cav1 or interpreted with caution if endogenous validation is not possible. Live imaging of cells expressing Cav1–GFP confirmed the increase in Cav1 spot intensity with the time of exposure to Cyt D (Fig. 4C). Clustering appeared to stem from the fusion or convergence of smaller spots (Fig. 4D; supplementary material Movie 1). Live imaging showed that only a fraction of spots is sensitive to Cyt-D-induced clustering (white circle in Fig. 4E; supplementary material Movie 2), while nearby spots were insensitive to treatment and did not cluster (green circles), and some moved out the TIRF plane (magenta circle). Simultaneous monitoring of Cav1–GFP and lifeact-labeled actin filaments (Riedl et al., 2008) by TIRF-m detected a pool of Cav1 spots close to actin fibers (Fig. 4, white arrows; supplementary material Movie 3). As the actin fibers depolymerized upon Cyt D treatment, Cav1 spots were dragged by the depolymerizing fibers, clustering into one bright spot that colocalized with actin accumulations (Fig. 4F; supplementary material Movie 3). These results suggest that Cav1 spots close to actin fibers are physically linked to them, and are clustered upon defective actin polymerization.

Interestingly, although dynamin2 knockdown inhibited Cav1 inward trafficking in detached cells (supplementary material Fig. S1G), it did not increase Cav1 spot clustering, and dim spots were more abundant (supplementary material Fig. S2E,F,H).

Together with the requirement of actin to initiate Cav1 inward trafficking (Fig. 1A–C), these results suggest that the actin-linked Cav1 pool may undergo inward trafficking upon loss of cell adhesion. To directly visualize actin and Cav1 during inward movement we induced partial cell rounding in attached cells. Under these conditions, Cav1 spots trafficked from the cell edge towards the perinuclear area, but slightly slower than in response to rapid detachment, and clear internal accumulation of Cav1 was evident only after 50 minutes (Fig. 4G). At this time, Cav1 spots showed a pattern similar to that of twisted actin fibers, frequently in bands parallel to the PM (Fig. 4G), suggesting that Cav1 remains bound to actin during its trafficking from the cell edge and that this is required for the initial stages of inward trafficking. In favor of this idea, patches of endogenous Cav1 and actin were evident in dRecAA cells but were not observed in dKOAA cells (Fig. 4H).

mDia1 regulates Cav1 inward trafficking and organization, the actin-linked Cav1 pool and caveolae formation

To investigate how Abl kinases regulate Cav1 inward trafficking we first focused on pY14Cav1. The levels of pY14Cav1 were similar in dRecAA and dKOAA cells at basal and H_2O_2-stimulated conditions (Fig. 5A), suggesting that Abl kinases use other effectors to regulate Cav1. The similarity between the phenotypes obtained by depletion of Abl kinases and actin disruption prompted us to test whether actin regulators downstream of Abl kinases are involved in Cav1 inward trafficking. The action of Abl tyrosine kinases in Cav1 inward trafficking is also independent of the Abl effectors N-WASP, cortactin and the Wave/Abi complex, which are actin regulators implicated in clathrin-mediated endocytosis (Boyle et al., 2007; Burton et al., 2003; Dai and Pendergast, 1995; Innocenti et al., 2005; Leng et al., 2005; Lommel et al., 2001), and do not regulate Cav1 inward trafficking (Fig. 5B–E,F,J). Similarly, independent knockdown of the essential Arp2/3 subunits p21Arc (Arpc3) and Arp3 (Actr3) did not interfere with Cav1 inward trafficking (Fig. 5G–J). Thus, despite the clear effect of Cyt D on Cav1 inward trafficking, Arp2/3-mediated actin reorganization is dispensable for this process.

Next, we focused on actin regulators of the formin family. In fruit flies, mutations in the formin diaphanous enhance the Abl mutant phenotype, suggesting that these genes genetically

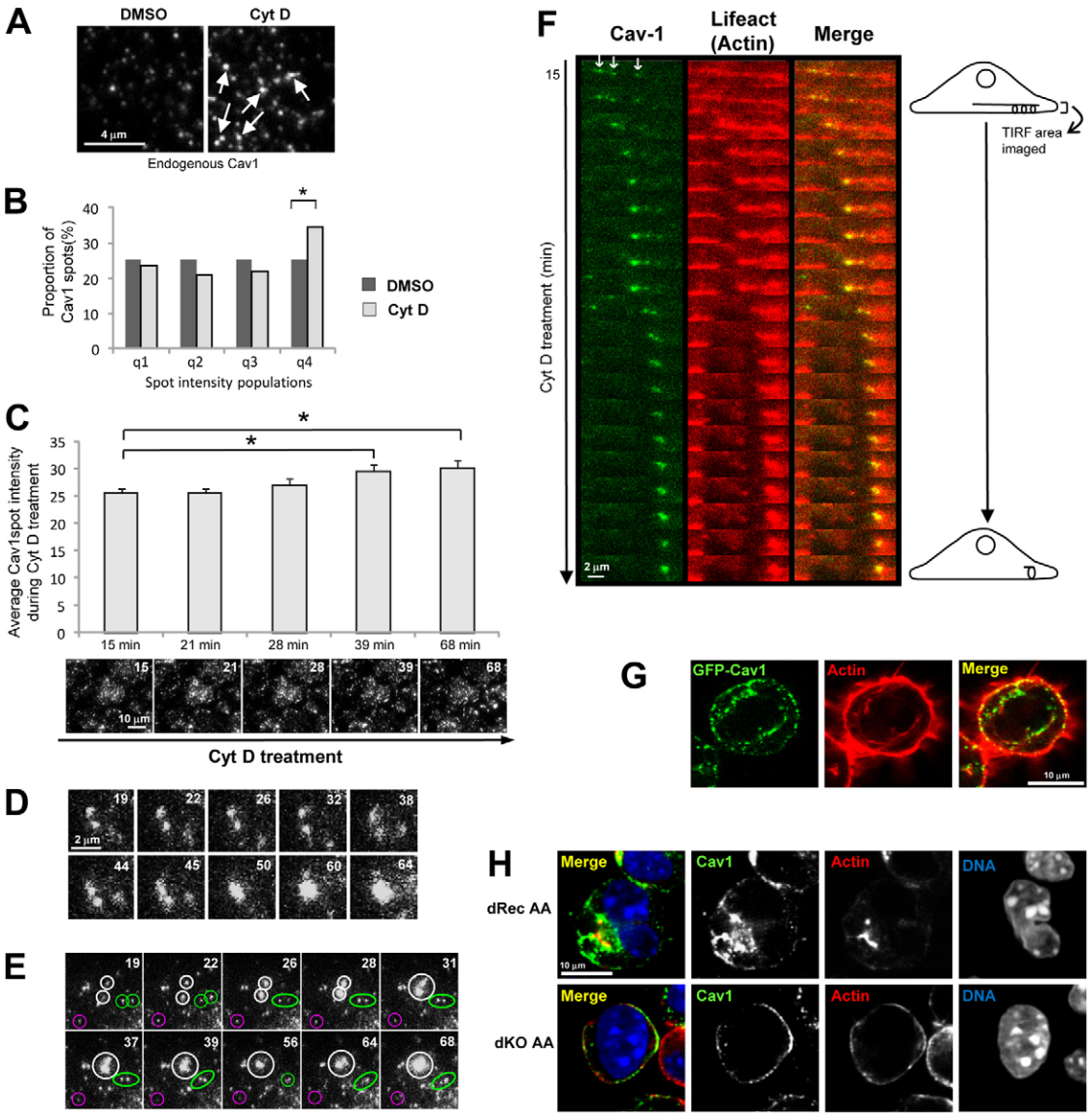

Fig. 4. The actin cytoskeleton organizes an actin-linked Cav1 pool involved in inward trafficking. (**A**) Endogenous Cav1 spot clustering induced by Cyt D. Representative TIRF-m images of Cav1–GFP spots in HeLa cells. White arrows mark bright Cav1 clusters formed after 40 minutes. (**B**) Bright endogenous Cav1 spots are increased upon Cyt D treatment. The Cav1 spot intensity values separated in four populations (q1 being the dimmest spots and q4 the brightest spots) are shown for DMSO- and Cyt-D-treated cells (40 minutes). *χ^2-test $P<10^{-5}$. (**C**) The effect of Cyt D on Cav1 clustering is cumulative. Spot size was recorded in the same group of cells from shortly after Cyt D addition. $n=166$–197. (**D**) Cyt-D-induced formation of large Cav1–GFP clusters occurs through convergence of two or more smaller spots. TIRF-m video recording of HeLa cells revealing convergence of Cav1–GFP spots with time (indicated in minutes in each frame) of Cyt D treatment. (**E**) Different pools of Cav1 spots have different sensitivities to actin disruption. In the TIRF-m video recording, Cyt D-induced Cav1–GFP clustering is observed for a small fraction of spots (white circles). Other nearby Cav1 spots were not affected (green circles), and others disappeared from the TIRF plane (magenta circles). Scale bar: 2 μm. (**F**) Cav1 spots are linked to the actin fibers and are clustered upon actin depolymerization. Cav1 spots and actin fibers were imaged by TIRF-m in HeLa cells expressing Cav1–GFP and the filamentous actin marker mRFP–Ruby–Lifeact from 15 to 68 minutes after Cyt D addition. The average separation between consecutive frames is 1.6 minutes. Three Cav1 spots (marked with arrows) are linked to the actin fiber and are dragged by the depolymerizing fiber until they cluster and colocalize with the actin marker. The process is represented in the cartoon. Orientation of the image was flipped 90°. (**G**) Internalized Cav1 follows a similar pattern to actin fibers. HeLa cells expressing Cav1–GFP were treated with tenfold diluted trypsin–EDTA and fixed when cells rounded up (50 minutes). Confocal images of Cav1–GFP and actin are shown. (**H**) Internalized endogenous Cav1 follows a similar pattern to actin patches. dRecAA and dKOAA cells were kept in suspension for 20 minutes and endogenous Cav1 and actin were examined by confocal microscopy.

interact (Grevengoed et al., 2003). Knockdown of mDia2 and formin1 had no significant effect on Cav1 perinuclear accumulation (Fig. 5K). However, these proteins are low expressed in HeLa cells (Fig. 5L, data not shown), suggesting that do not play a major role in this process.

In contrast, depletion of mDia1 reproduced the effects of c-Abl+Arg depletion and Cyt D. Perinuclear accumulation of endogenous Cav1 was reduced by about 40% (Fig. 6A,B,D). This was reproduced with Cav1–GFP as a readout (supplementary material Fig. S3A,B,D). Off-target effects were excluded with

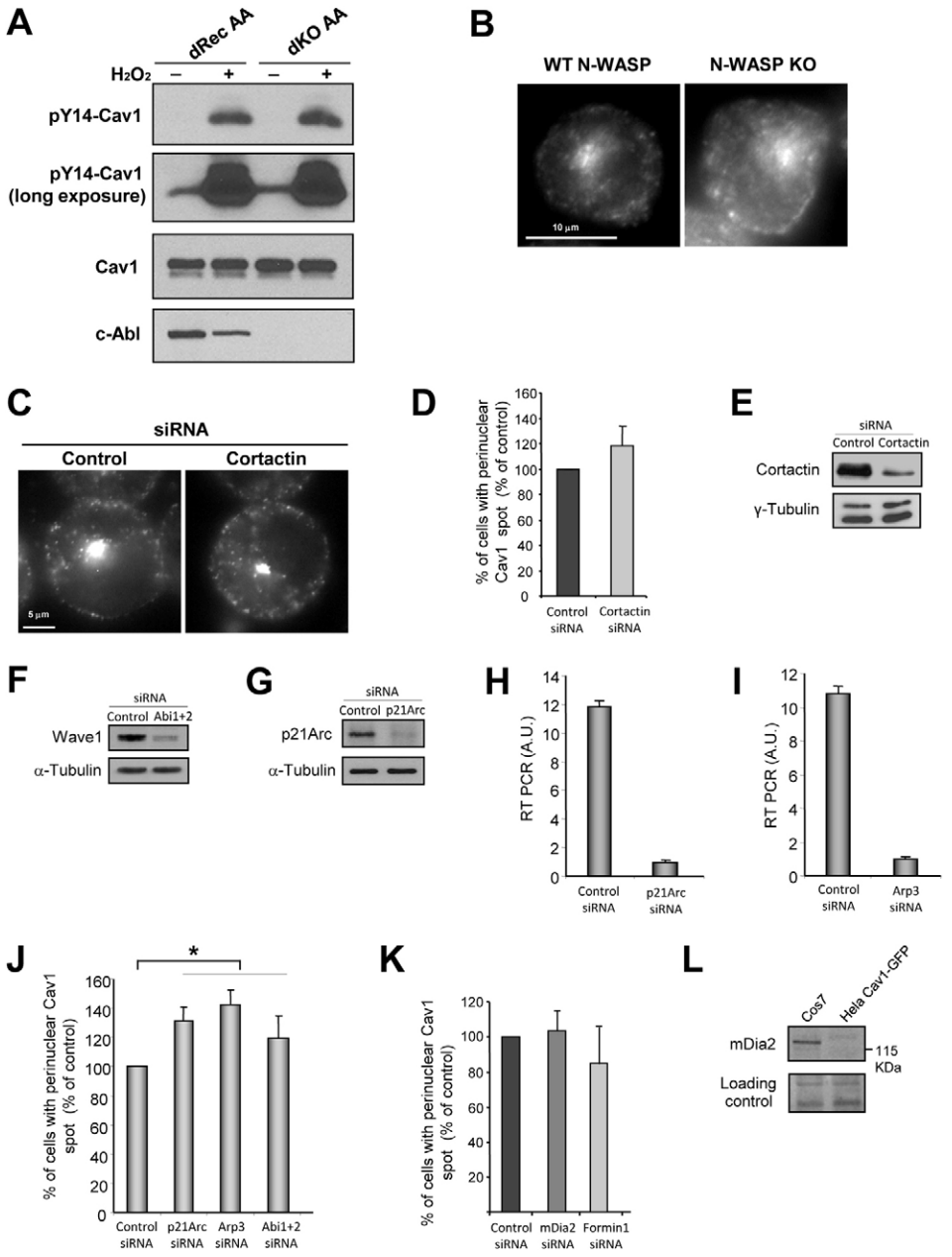

Fig. 5. PhosphoY14-Cav1 in c-Abl/Arg KO MEFs and the effect of lack of N-WASP, cortactin, Abi1+2, Arp2/3, mDia2 and formin1 on detachment-induced Cav1 inward trafficking. (**A**) pY14 Cav1 levels were similar in Abl-kinase-deficient cells and control cells. Control and H_2O_2-treated cells (5 mM for 5 minutes) were lysed in RIPA and cell lysates were blotted using the indicated antibodies. (**B**) Absence of N-WASP does not reduce the rate of Cav1 trafficking. Wild-type (WT) or N-WASP KO cells were placed in suspension for 120 minutes and stained for endogenous Cav1. (**C**) HeLa cells expressing Cav1–GFP were transfected with control or cortactin siRNA, placed in suspension, fixed and imaged for Cav1–GFP. (**D**) Quantification of spot-like perinuclear accumulation of Cav1–GFP in cells as in C. (**E**) Immunoblot showing specific suppression of cortactin in HeLa Cav1–GFP cells transfected with cortactin siRNA. γ-Tubulin was detected as a loading control. (**F**,**G**) Immunoblots showing specific suppression of Wave1 and p12Arc in Cav1–GFP-expressing HeLa cells transfected with Abi1+Abi2 or p12Arc siRNAs. Abi1+Abi2 knockdown was assessed by blotting for Wave-1, which is degraded in the absence of Abi1 and Abi2. α-tubulin was detected as a loading control. (**H**,**I**) Quantitative RT-PCR of target mRNA expression in Cav1–GFP-expressing HeLa cells transfected with p21Arc or Arp3 siRNAs. (**J**) Quantification of perinuclear Cav1–GFP in HeLa cells transfected with control, p21Arc, Arp3 or Abi1+2 siRNAs. Cells were placed in suspension for 60 minutes, and spot-like localization of Cav1–GFP in the perinuclear area was monitored blind. $n>4$. (**K**) Quantification of spot-like perinuclear accumulation of Cav1–GFP in HeLa cells transfected with control, mDia2 or formin1 siRNAs. (**L**) Immunoblot showing expression of mDia2 protein in HeLa cells expressing Cav1–GFP and in Cos7 cells.

two additional mDia1 siRNAs (supplementary material Fig. S3B,E). mDia1 silencing prevented internalization of the cell-edge endogenous Cav1 pool within the first 20 minutes after detachment (Fig. 6A,C), and Cav1 internalized at later stages remained at the periphery (Fig. 6A,C). Similar results were obtained with Cav1–GFP (supplementary material Fig. S3A,C). Furthermore, cells silenced for mDia1 showed a ~15% reduction in plasma membrane GM1 levels during suspension time, which was significantly lower than control siRNA transfected cells (~36%; Fig. 6E). mDia1 depletion also induced clustering of endogenous Cav1 PM spots in attached cells (Fig. 6F). The percentage of bright Cav1 spots (q4 population) was increased by ~25% (Fig. 6G). Similar to Abl kinase silencing, mDia1 depletion induced an increase in clustered caveolar domains observed by EM (Fig. 2D,F), correlating with an increase in Cav1 clustering observed in immunofluorescence images (Fig. 6F). In addition, mDia1 silencing increased the amount of Rac1 at the leading edge of spreading cells (Fig. 6I,J).

Like Abl silencing, mDia1 knockdown did not inhibit Cav1 z-movement (Fig. 6H). Unlike the effect of disrupting the c-Abl or mDia1, Arp3 knockdown had no significant effect on Cav1 spot clustering at the basal membrane (supplementary material Fig. S2I,J). Actin disruption and suppression of Abl kinases and mDia1 expression thus have similar effects on Cav1 organization and inward trafficking that are opposite to those observed upon Arp2/3 silencing.

To test the effect of mDia1-induced actin remodeling on Cav1 dynamics, we transfected HeLa cells with constitutively active mDia1ΔN3, which induces a parallel array of actin fibers and stable microtubules (Ishizaki et al., 2001; Palazzo et al., 2001). Endogenous Cav1 (but not EEA-1) in mDia1ΔN3-expressing cells strongly co-aligned with stress fibers (Fig. 7A,B,D,E),

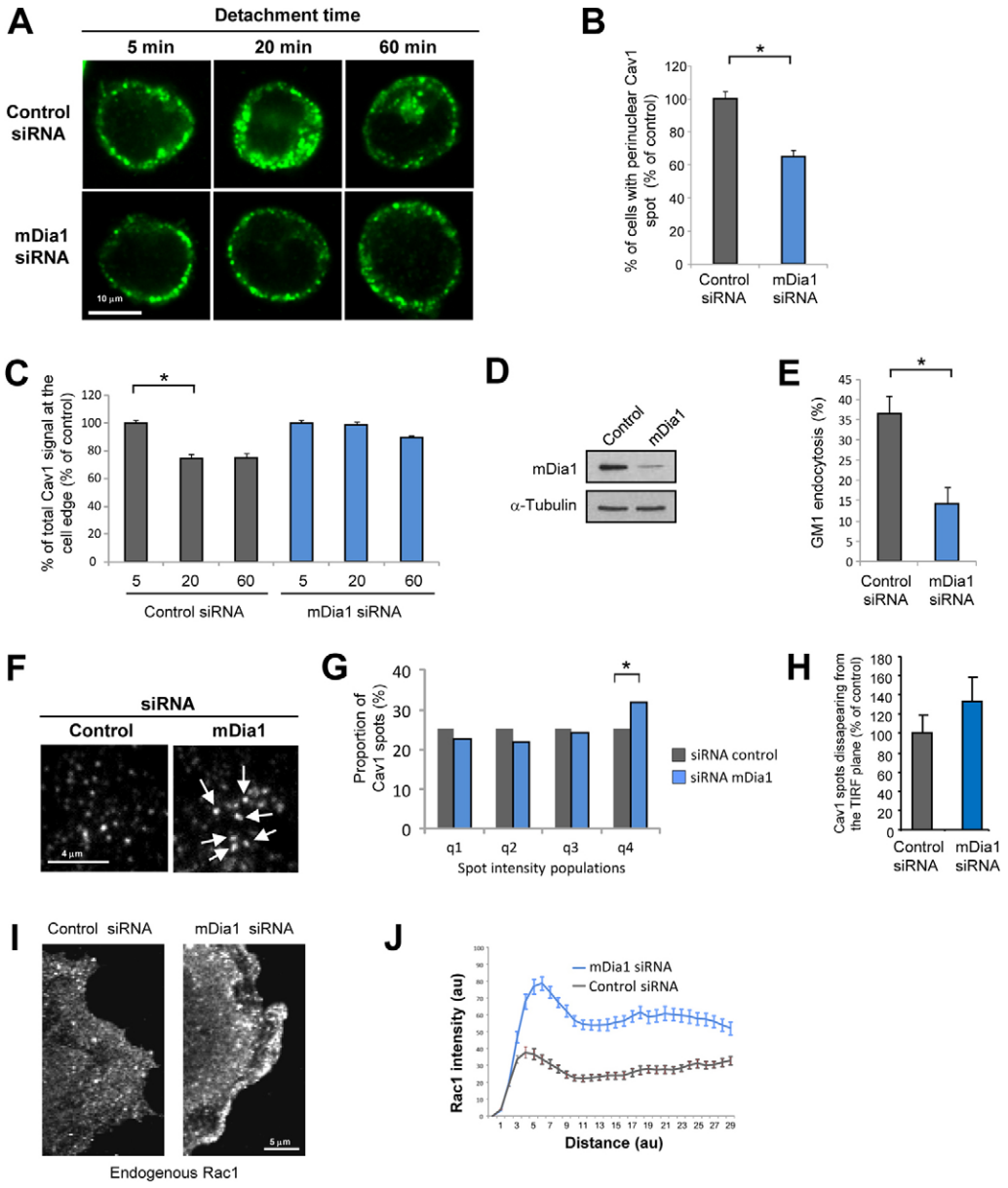

Fig. 6. mDia1 regulates Cav1 spatial organization and inward trafficking but not z-movement. (**A**) Knockdown of mDia1 blocks endogenous Cav1 inward trafficking. HeLa cells transfected with control or mDia1 siRNAs were placed in suspension, fixed and stained at the indicated times. Images show representative confocal sections taken at the cell equator. (**B**) Quantification of the internal endogenous Cav1 pool in detached cells as in A. HeLa cells were transfected with control or mDia1 siRNAs, and perinuclear Cav1 accumulation was blind-scored after suspension for 60 minutes. $n=3$. (**C**) Quantification of the cell-edge endogenous Cav1 pool in cells as in A. The amount of Cav1 at the cell edge was normalized to the total amount of Cav1 in each cell. Data are normalized to 5 minutes after detachment. Note that cell-edge Cav1 is not significantly reduced after the first 20 minutes in mDia1-depleted cells. $n=96$–190. (**D**) Immunoblot showing suppression of mDia1 expression in HeLa cells transfected with mDia1 siRNA. (**E**) Endocytosis of GM1 is reduced in mDia1-silenced cells. SiRNA-transfected cells were plated on a fibronectin-coated surface 24 hours before the assay. Cells were kept in suspension for 0.25 or 60 minutes, then placed at 4℃, and cell-surface-bound CTB–Alexa-Fluor-647–GM1 complex was quantified by FACS. Endocytosis of GM1 was calculated as the percentage drop in surface GM1 levels after the suspension period. $n=3$. (**F**) siRNA knockdown of mDia1 in HeLa cells induces formation of bright endogenous Cav1 spots. Representative TIRF-m images are shown. White arrows mark bright Cav1 clusters. (**G**) Bright endogenous Cav1 spots are increased in mDia1-silenced cells. The Cav1 spot intensity values were separated in four populations (q1 being the dimmest spots and q4 the brightest spots). *χ^2-test $P<10^{-5}$. (**H**) Cav1 z-movement is not positively regulated by mDia1. Disappearance of Cav1–GFP spots from the TIRF plane was measured as indicated in the Materials and Methods. (**I**) Plasma membrane targeting of endogenous Rac1 is regulated by mDia1. Immunofluorescence of endogenous Rac1 in control or mDia1-silenced cells allowed to spread on fibronectin (10 μg/ml) for 40 minutes. (**J**) Quantification of the average intensity of Rac1 staining in each pixel from the cell exterior to the cytoplasm. Intensity measurements were taken from 10 points on the cell edge and a line was drawn to the cell interior. Mean intensity values ± s.e.m. are shown at each position (in pixels); $n=30$ and 21.

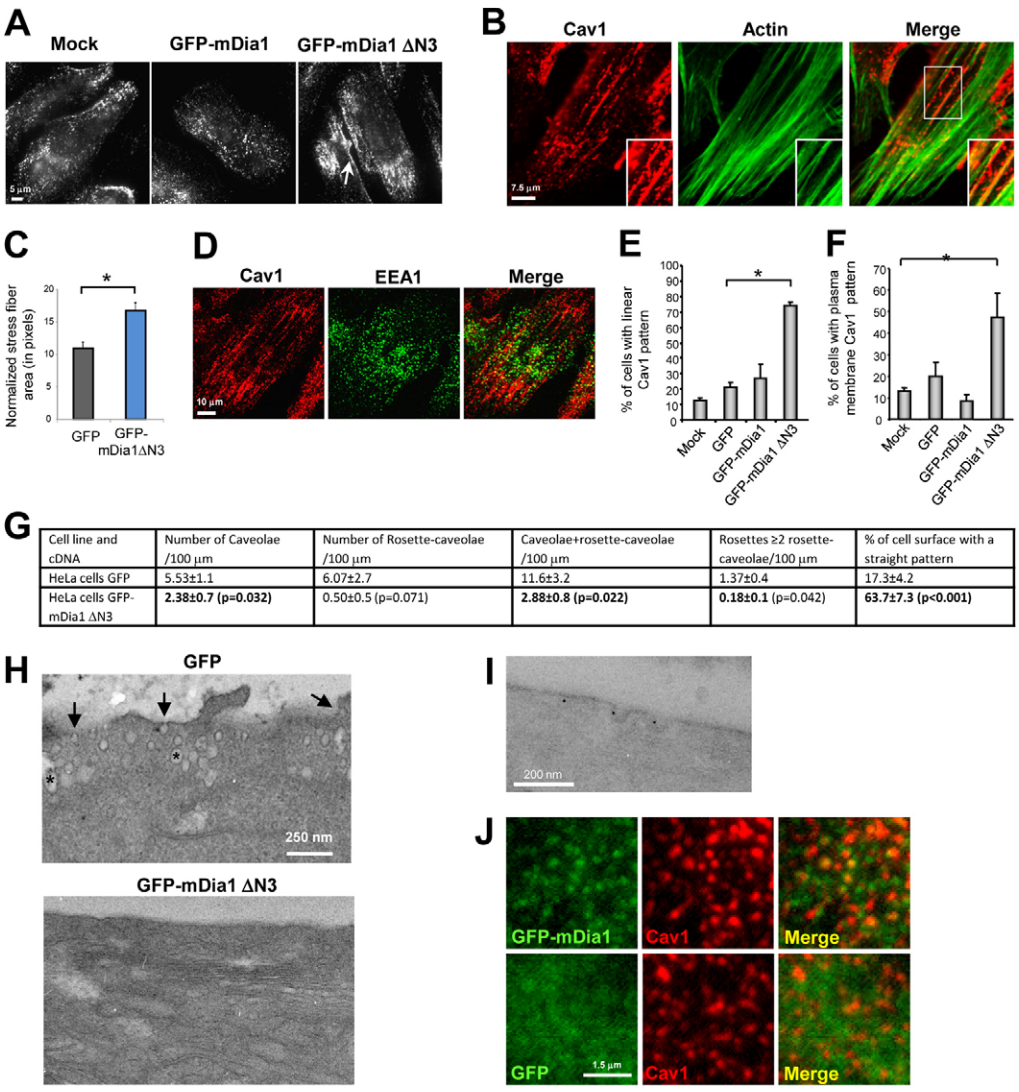

G

Cell line and cDNA	Number of Caveolae /100 μm	Number of Rosette-caveolae /100 μm	Caveolae+rosette-caveolae /100 μm	Rosettes ≥2 rosette-caveolae/100 μm	% of cell surface with a straight pattern
HeLa cells GFP	5.53±1.1	6.07±2.7	11.6±3.2	1.37±0.4	17.3±4.2
HeLa cells GFP-mDia1 ΔN3	**2.38±0.7 (p=0.032)**	0.50±0.5 (p=0.071)	**2.88±0.8 (p=0.022)**	**0.18±0.1** (p=0.042)	**63.7±7.3 (p<0.001)**

Fig. 7. mDia1 activity regulates the actin-linked Cav1 pool and caveolae flattening. (**A**) Immunofluorescence of endogenous Cav1 in HeLa cells transfected with mDia1 or active mDia1ΔN3. The white arrow indicates the pool of Cav1 at the PM. (**B**) HeLa cells expressing mDia1ΔN3 were stained for actin and Cav1. Enlarged images (insets) show contrast- and brightness-enhanced views of the area of alignment of Cav1-positive spots and stress fibers. (**C**) Stress fibers are increased in mDia1ΔN3-expressing cells. Stress fiber area was normalized to the total analyzed area in each cell. $n=33$ and 77. (**D**) HeLa cells expressing mDia1ΔN3 were stained for EEA-1 and Cav1. (**E**) Percentage of cells transfected as in A showing a linear array pattern of Cav1 staining. $n=4$. (**F**) Percentage of cells transfected as in A showing a PM pattern of Cav1 staining. $n=3$. (**G**) Active mDia1 reduces the amount of caveolae and caveolar rosettes. Quantification of caveolar domain structures imaged with EM in GFP- or GFP–mDia1ΔN3-transfected cells. Average straightness of each set of cells is also shown. Student's two-tailed *t*-test *P*-values are shown in brackets and shown in bold if below 0.05; $n>10$. A total of 553.8 μm (GFP) and 554.3 μm (GFP–mDia1ΔN3) was analyzed. Data are representative of two independent experiments. (**H**) Active mDia1 reduces the amount of caveolae and caveolar rosettes. Electron micrographs of HeLa cells transfected with GFP or GFP–mDia1ΔN3. Morphologically defined caveolae (arrows) and caveolar rosettes (asterisks) are marked. (**I**) Electron micrographs of GFP–mDia1ΔN3-expressing HeLa cells processed for immunogold labeling of endogenous Cav1. Visualization of caveolae is impaired by this method, but note the increased width of the caveolae necks. (**J**) HeLa cells were transfected with GFP–mDia1 or GFP and stained for endogenous Cav1. The panels show representative TIRF micrographs of fixed cells. Note the punctate pattern of GFP–mDia1 staining, reflecting association with the tips of actin filaments (Higashida et al., 2004).

suggesting that the actin polymerization induced by mDia1ΔN3 holds Cav1 spots in tight association with the actin cytoskeleton (Fig. 7B, enlarged area). Under these conditions active mDia1 increased the amount of stress fibers, which might explain the Cav1 distribution phenotype (Fig. 7C).

In addition to spot alignment with actin fibers, Cav1 was increased at the cell edge, and the characteristic PM staining of Cav1 was significantly increased upon mDia1ΔN3 expression (Fig. 7A, white arrows, quantified in 7F). EM and immunogold-EM, to respectively detect caveolar domains and Cav1, indicated that cells expressing active mDia1 had fewer PM caveolae and caveolar rosettes than GFP-expressing control cells (Fig. 7G,H). The effect of this mutant was also evident in the cell shape, that was straighter than in control cells (Fig. 7A,G). While active mDia1 induced cell elongation (Watanabe et al., 1999) and straightness, and this correlated with lower caveolae and rosette density, we did not observe a clear correlation between the location of individual caveolae and the straightness on the surrounding PM

(data not shown). Although there were fewer caveolae in mDia1ΔN3-expressing cells, immunofluorescence staining suggested that there was more Cav1 at the PM (Fig. 7A,F). To elucidate this point, we used immunogold-EM to detect Cav1 at regions within defined distances from the PM. Consistent with the immunofluorescence data (Fig. 7A), mDia1ΔN3-expressing cells contained ~30% more gold particles than control cells in the region closest to the PM (0–50 nm; 67.1/100 vs 44.7/100, gold particles/100 μm of PM analyzed). Given that transfection efficiency was ~70%, these data might underestimate the effects of mDia1ΔN3.

These results suggest that active mDia1 might induce the disappearance of caveolae while preserving Cav1 at the PM; this apparent paradox could be a consequence of the cortical stiffness of the cell membrane (Tamura et al., 2010) and cell elongation (Watanabe et al., 1999) induced by this mutant mDia1, which would flatten caveolae (Sinha et al., 2011). Consistently, although immunogold-EM often hampers visualization of caveolae, the few caveolae observed appeared to have wider necks (Fig. 7I). Similarly, the numbers of small caveolar rosettes observed in adherent cells was decreased upon expression of active mDia1 (Fig. 7G,H), suggesting that they are sensitive to disassembly upon cell elongation induced by an excess of stress fibers. Overexpression of wild-type mDia1 (Fig. 7A,E,F) or individual FH1 and FH2 domains (data not shown) had no obvious effect on Cav1 staining or cell elongation (Ishizaki et al., 2001), strongly suggesting that the action of mDia1ΔN3 is dependent on its actin nucleation or microtubule stabilizing activities. Cyt D, but not nocodazole, completely abrogated the linear arrangement of Cav1 and its PM localization in mDia1ΔN3-expressing cells (supplementary material Fig. S4A–C). The slight effect of nocodazole on Cav1 PM localization (supplementary material Fig. S4C) probably reflects a microtubule-based recycling of Cav1 to the PM induced by active mDia1 (Wickström et al., 2010). GFP–mDia1 is known to localize at the tips of actin fibers (Higashida et al., 2004). TIRF–m showed that a significant fraction of GFP–mDia1 can target and colocalize with endogenous Cav1 (approximately sevenfold over control GFP; Fig. 7J).

Abl kinases regulate Cav1 association to stress fibers and inward trafficking through an mDia1-dependent mechanism

The similar phenotypes of cells depleted of Abl tyrosine kinases and mDia1 suggest that these proteins might act in the same pathway upstream of Cav1 organization and trafficking. We found that expression of active FLAG-tagged mDia1, which induced significant co-alignment of Cav1 patches with stress fibers (Fig. 7A,B,E), restored the actin-fiber co-aligned Cav1 pool (Fig. 8A,B,E), and most importantly fully rescued (~79% of cells) the trafficking of Cav1 to the perinuclear area in dKOAA cells (Fig. 8C–E). Active RhoAV14 also rescued trafficking in dKOAA cells but very inefficiently (29±5.6% of cells with perinuclear Cav1 in RhoV14 expressing cells versus ~20% in control cells), suggesting that RhoA is not downstream of Abl kinases, and that these kinases act mostly downstream or independently of RhoA. TIRF-m analysis in HeLa cells revealed colocalization of active c-Abl with mDia1 at the basal PM, and most c-Abl-labeled structures were positive for mDia1 (Fig. 8F); similar results were obtained with GFP–c-Abl and Cherry–mDia1 (supplementary material Fig. S4D). A fraction of the c-Abl and mDia1 positive patches were positive for endogenous Cav1 (Fig. 8F). Although constitutively active c-Abl was able to weakly phosphorylate overexpressed mDia1 (supplementary material Fig. S4E), we could not detect endogenous tyrosine-phosphorylated mDia1. Moreover, mutation of mDia1 all 19 tyrosine residues (alone and in various combinations) had no clear effect on mDia1 localization or phosphorylation by Abl kinases and we did not consistently detect any phosphorylated residue by mass spectrometry (data not shown). Abl tyrosine kinases thus appear to regulate Cav1 organization and trafficking via an mDia1-dependent mechanism but independently of direct mDia1 phosphorylation.

Discussion

Caveolae are organized at different levels of complexity, from flattened caveolae to large rosettes, but caveolar organization and trafficking is still poorly understood. Several studies suggest that the actin cytoskeleton is implicated at some level in caveolae biology. A tight association of Cav1 or caveolae with actin filaments has been described (Kanzaki and Pessin, 2002; Morone et al., 2006; Muriel et al., 2011; Pelkmans et al., 2002; Richter et al., 2008; Rothberg et al., 1992; Stahlhut and van Deurs, 2000). This may occur through an actin and caveolae binding complex that can be detected by EM (Richter et al., 2008), and in which filamin A may play an active role (Muriel et al., 2011; Stahlhut and van Deurs, 2000). In addition, distinct effects of actin disrupting drugs on Cav1 motility and caveolae endocytosis have been described (Kang et al., 2000; Mundy et al., 2002; Parton et al., 1994; Pelkmans et al., 2002; Thomsen et al., 2002). Our results show that an Abl kinase-governed pathway upstream of mDia1 regulates Cav1/caveolae organization and Cav1 inward trafficking through actin stress fibers.

Abl tyrosine kinases play a major role in caveolae organization and trafficking. In attached cells, deficiency of these kinases results in a deficient spatial organization of caveolae, which instead of being aligned with actin stress fibers are organized into small clusters. Upon loss of tension triggered by loss of cell adhesion, large and complex caveolar rosettes are formed that precede Cav1 inward trafficking to the perinuclear area. These two sequential events are impaired in the absence of Abl kinases, suggesting that the deficient organization of caveolae/Cav1 observed in attached conditions in Abl-deficient cells prevents the adequate formation of caveolar rosettes upon loss of cell adhesion, impairing Cav1 inward trafficking. Mechanistically, Abl kinases organize caveolar domains through their action on stress fibers. Despite the abundance of Abl kinase effectors that regulate the actin cytoskeleton (Colicelli, 2010), mDia1 silencing mimics Abl depletion phenotypes in terms of Cav1 organization and trafficking, and active mDia1 rescues the actin co-aligned Cav1 pool and Cav1 inward trafficking in Abl/Arg KO cells. This suggests that the actin–Cav1 axis regulated by mDia1 determines the subsequent Cav1 trafficking regulated by Abl kinases. However, Abl kinases appear to indirectly regulate mDia1 activity and localization (Grevengoed et al., 2003), consistent with our inability to detect endogenously tyrosine phosphorylated mDia1. It is therefore likely that Abl kinases target other players which in turn regulate mDia1-mediated stress fiber formation.

Our findings assign a key role to mDia1 regulated stress fibers in the organization and trafficking of caveolar domains. The importance of stress fibers in caveolar domain organization is reinforced by the ability of active mDia1 to target Cav1 to the

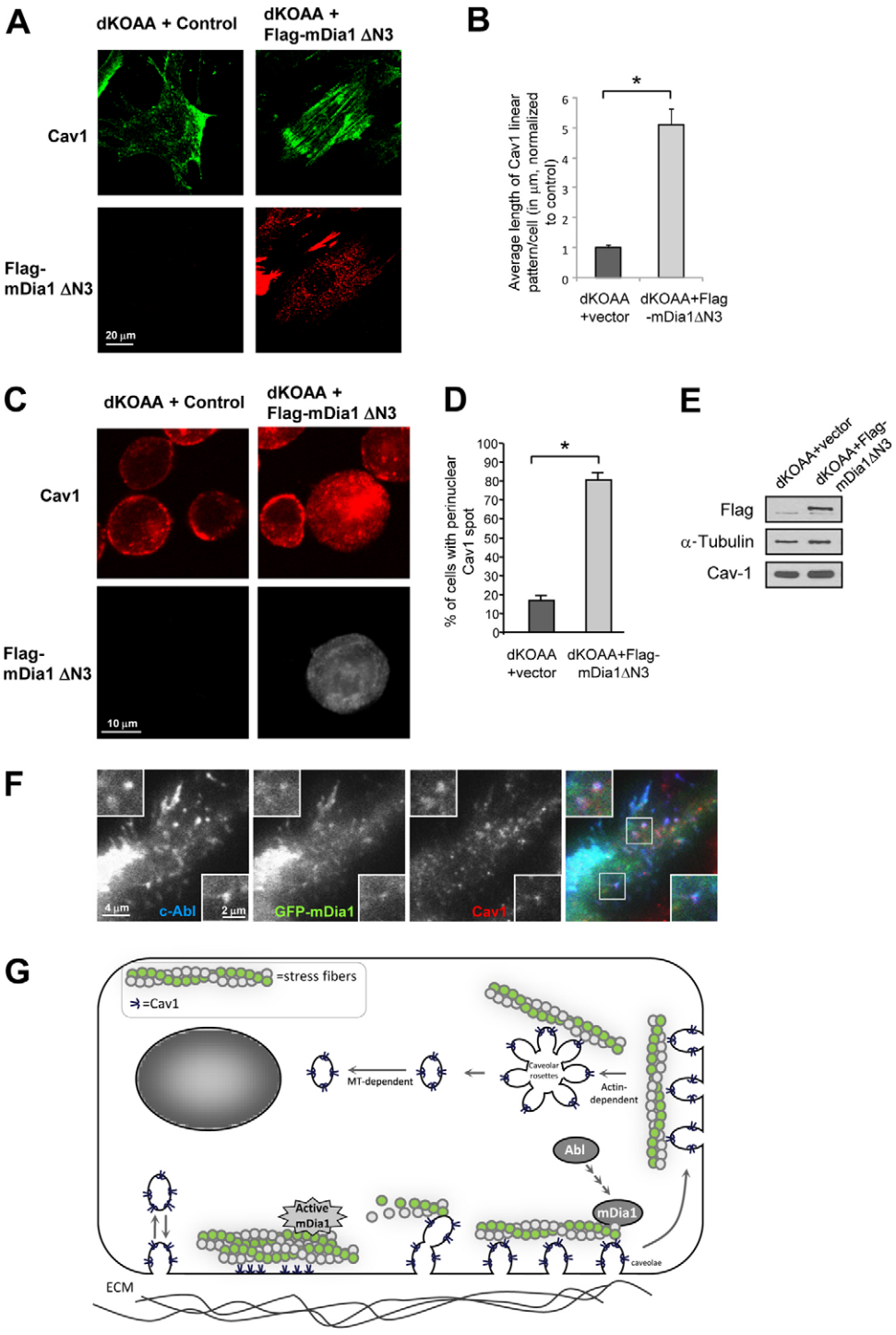

Fig. 8. Active mDia1 rescues Cav1 inward trafficking in cells deficient for Abl kinases. (**A**) Linear distribution of Cav1 is restored in dKOAA cells upon expression of active mDia1. dKOAA MEFs infected with control- or FLAG–mDia1ΔN3-expressing virus were plated on fibronectin-coated surfaces and stained for Cav1 and FLAG–mDia1ΔN3. (**B**) Quantification of linear Cav1. The length of each Cav1 line was measured blind and the total length was summed for each cell. $n=218$ and 37. (**C**) Active mDia1 rescues Cav1 inward trafficking in dKOAA cells. dKOAA cells were infected with a retrovirus expressing active FLAG–mDia1ΔN3 or a control retrovirus. Cells were placed in suspension for 60 minutes and immunostained for endogenous Cav1 and FLAG–mDia1ΔN3. Only cells expressing FLAG–mDia1ΔN3 were able to induce proper endogenous Cav1 inward trafficking. Representative confocal immunofluorescence micrographs are shown. (**D**) Quantification of internal Cav1 in mock-infected and FLAG–mDia1ΔN3-expressing dKOAA cells. $n=4$. (**E**) Protein expression of FLAG–mDia1ΔN3, α-tubulin and Cav1 in mock-infected and FLAG–mDia1ΔN3-expressing dKOAA cells. (**F**) c-Abl, mDia1 and Cav1 partially colocalize at the PM or very close to it. HeLa cells transfected with GFP–mDia1 and active c-Abl were stained for c-Abl and endogenous Cav1 and analyzed by TIRF-m. Insets show enlarged views of the boxed areas. (**G**) Proposed model of the role of Abl and mDia1 in regulating the spatial organization of Cav1/caveolae and its inward trafficking upon loss of cell adhesion (represented as the non-adherent areas of the cell). A pool of caveolae/Cav1 linked to stress fibers is regulated by Abl kinases and mDia1, and correct association with actin fibers is required to form surface-connected caveolar rosettes and initiate Cav1 inward trafficking upon loss of cell adhesion. Induction of stress fibers by active mDia1 induces caveolar flattening. The regulation of mDia1 by Abl kinases is most probably indirect, as indicated by repeated arrows. A second pool of Cav1 vesicles undergoing rapid z-movement at the basal membrane is not regulated by this pathway.

PM, align it with actin, and reduce caveolae and caveolar rosette density. The increase in stress fiber content and cell size, elongation and cortical stiffness induced by this protein (Tamura et al., 2010; Watanabe et al., 1999) might be responsible for caveolar domain flattening. In fact, both mechanical cell stretching and cell swelling upon hypo-osmotic treatment also cause caveolae flattening and disassembly (Sinha et al., 2011). These studies raised the possibility that actin-fiber-borne membrane tension (Hayakawa et al., 2011) might be transmitted to caveolar domains. Upon loss of cell adhesion the stress fibers are altered, which might contribute to the reported loss of membrane tension (Colbert et al., 2009) and to the increase in caveolar complexity (rosette formation) observed under these conditions. Other studies have also reported that changes in surface remodeling and cell volume are associated with caveolar complexity and/or inward trafficking. Parton and colleagues observed that the formation of large rosettes and Cav1 internalization were induced in response to hyperosmotic + okadaic acid conditions, which reduces the cell volume (Parton et al., 1994). Similarly, Cav1 initiates inward trafficking during

mitosis (Boucrot et al., 2011), and caveolar rosettes are abundant in non-adherent areas of attached adipocytes (Parton et al., 2002). The opposite effect is observed when cells need to significantly extend their surface such as upon cell spreading, during which Cav1 is recycled to the PM (del Pozo et al., 2005). In fact, cavin1 and Cav3 have been implicated in membrane repair (Cai et al., 2009; Zhu et al., 2011). Thus, changes in the ratio of cell surface area to cell volume and in tension might regulate the organization and trafficking of caveolar domains. In this context, it is feasible to envision that stress fibers might actively regulate the organization of caveolar domains, since they are tightly coupled to adhesion receptors (Parsons et al., 2010) and to the plasma membrane (Morone et al., 2006). In this scenario, Abl kinase activation by integrins (Lewis et al., 1996) and mDia1 localization to integrin complexes (Butler et al., 2006) could impinge locally on caveolae organization and dynamics by modulating actin fibers. It is further possible that the role of integrins (Vogel and Sheetz, 2006) and mDia1 (Chan et al., 2010) in mechanotransduction could be coupled to force-induced caveolar domain organization (Sinha et al., 2011). The tension sensing ability of actin filaments (Hayakawa et al., 2011) might also be transmitted to caveolar domains. Over 90% of caveolae are bound to actin filaments (Morone et al., 2006), which would facilitate a direct response to changes in actin filaments.

Although formation of caveolar rosettes precedes trafficking of Cav1 to the perinuclear area, it is still unclear whether caveolar rosettes themselves pinch off and traffic to the perinuclear area. Caveolar rosettes were infrequent in cells detached for 60 minutes, and we were unable to consistently detect rosettes not connected with the cell surface (ruthenium red negative) at time points of 5 minutes or longer (data not shown). This suggests that they do not traffic as a unit, and therefore that caveolar domains pinch off from the rosette; alternatively, they might traffic but be undetectable after a possible loss of the typical caveolar shape. The involvement of dynamin-2 in the perinuclear accumulation of Cav1 suggests that caveolar domains pinch off at some point shortly after loss of cell adhesion. In any case, caveolar rosettes appear to play an active role at the initial stages of the trafficking route, as supported by the absence of rosettes upon loss of cell adhesion in Abl-deficient cells, in which Cav1 trafficking is impaired.

The requirement for Abl, dynamin2 and mDia1 in Cav1 inward trafficking in detached cells contrasts with the unexpected lack of involvement of these molecules in the z-movement of Cav1 observed by TIRF-m in attached cells. These two types of Cav1 movement occur under different conditions – attached versus detached – which might explain the different requirements. Different caveolar pools exist in attached cells, one pool being static while the other is highly mobile (z-movement) (Pelkmans and Zerial, 2005). Different linkage of these pools to actin filaments could determine their differential regulation and mobile characteristics. This idea is supported by the increased mobility of the Cav1 static pool observed upon Cyt D treatment (Thomsen et al., 2002), which suggests that the static pool, but not the highly mobile pool, is bound to actin. This could explain why Abl and mDia1 only affect the movement of Cav1 in suspended cells, where the actin-linked pool undergoes inward movement, while the free and rapidly moving pool observed in attached cells is independent on this pathway.

The involvement of Cav1 trafficking in the regulation of pathways that contribute to anoikis, such as the Erk–MAPK, PI3K–Akt and Rac1–PAK pathways, has been previously shown (Cerezo et al., 2009; del Pozo et al., 2005; Reginato et al., 2003; Zhan et al., 2008) and highlights the importance of membrane remodeling during adhesion/de-adhesion cycles. Our results show that Abl kinases and mDia1 contribute to the downregulation of Rac1 from the leading edge, similar to Cav1 (Goetz et al., 2011). This regulation results in resistance to anoikis in anchorage independent growth (Cerezo et al., 2009), which could explain the strong downregulation of Cav1 levels induced by oncogenic forms of c-Abl kinase and other oncogenes (Koleske et al., 1995).

Together, the phenotypes reported here support a model (Fig. 8G) in which stress-fiber-linked caveolae are organized by a cassette composed of Abl tyrosine kinases and mDia1. The decrease in the number of stress fibers obtained by depletion of Abl or mDia1 results in clustering of caveolae. This prevents the formation of large caveolar rosettes in non-adherent areas of the cell that are required for perinuclear accumulation of Cav1. Thus, the spatial organization of caveolae dictated by stress fibers is needed to form large caveolar rosettes when adhesion is lost. Stress fibers also control caveolae flattening, since an excess of actin fibers induced by active mDia1 leads to caveolae flattening. A second pool of Cav1, undergoing z-movement at the basal membrane, is insensitive to Abl and mDia1. Thus, the ability of actin-linked caveolae to undergo flattening or form rosettes might be responsible for mechanosensing and/or mechanotransducing the inputs of adhesion and stress fiber regulatory pathways, which play a major role in mechanotransduction (Sinha et al., 2011; Vogel and Sheetz, 2006).

Materials and Methods

Plasmids, cells and reagents

FLAG–mDia1ΔN3 (mouse amino acids 543–1192) was cloned into the bicistronic GFP-expressing retroviral vector pRV-IRES CopGreen BglII site. GFP–mDia1 and mDia1ΔN3 expression vectors were as described (Ishizaki et al., 2001). c-Abl was cloned into pEGFPC2 EcoRI sites. mDia1 was cloned into BglII/SalI sites of pCherryC1. pmRFPRuby-N1-Lifeact was kindly provided by Roland Wedlich-Soldner (Riedl et al., 2008). Plasmids encoding active c-AblPP were as described (Barilá and Superti-Furga, 1998). All cells were grown in DMEM with 10% fetal bovine serum. c-Abl/Arg double knockout MEFs reconstituted with c-Abl+Arg or empty vector were kindly provided by Tony Koleske (Yale University, CT) and Ann Marie Pendergast (Duke University, NC) (Plattner et al., 2003). 293T/17 and HeLa cells were purchased from ATCC. HeLa cells expressing Cav1–GFP were kindly provided by Lukas Pelkmans (ZTH, Zurich), and cells expressing low levels of GFP were selected by Fluorescence-activated cell sorting (FACS). Polyclonal antibodies: caveolin (BD), mDia2 and Arg (H-300) (Santa Cruz). Monoclonal antibodies: c-Abl (8E9), mDia1, pTyr14-Cav1 and p21Arc (BD); 4G10 and Rac1 (Millipore); α-tubulin, FLAG M2 and γ-tubulin (Sigma). siRNA oligonucleotide sequences are described in supplementary material Table S1 and were purchased from Dharmacon, Qiagen and Ambion. As control non-targeting siRNAs, control #1 (Dharmacon) was used. Cyt D and nocodazole were used at 1.25 μM and 10 μM, respectively.

Immunoprecipitation, transfections and infections

Plasmids were transfected using fugene6. Transfection with siRNAs at 50/100 nM was done with Oligofectamine. Immunoprecipitations, immunofluorescence and retrovirus production and infection were as described (Echarri et al., 2004).

Adhesion-regulated Cav1 inward trafficking

Adhesion-regulated Cav1 inward trafficking assays were as previously described (del Pozo et al., 2004). Briefly, cells were trypsinized and transferred to methylcellulose solution [0.5% (w/v) methylcellulose, 0.2% (w/v) lipid free bovine serum albumin, and 0.5 mg/ml soybean trypsin inhibitor]. Cells were rotated at 37℃ for the indicated times. Typically, 25–35% of Cav1–GFP expressing HeLa cells showed spot-like perinuclear Cav1–GFP accumulation after 1 hour in suspension. At least 200 cells were scored blindly for each sample.

Microscopy and image analysis

Images were taken with a Zeiss Axiovert 200 M SP LSM5 (epifluorescence), a Leica TCS SP5 (confocal) and a Leica AM TIRF MC (TIRF) with a 100×, 1.46

NA objective. TIRF microscopy (TIRF-m) was used at a penetration depth of 90 nm. For TIRF-m movies of Cav1–GFP-expressing cells, a picture was acquired every 0.3 seconds with a peltier cooled (−75℃) Andor iXON EMCCD camera, producing a ~3.2-minute movie. Typically each movie contained about three to five randomly selected cells. To quantify Cav1–GFP disappearance events, cropped movies were played and disappearing objects were manually scored blind. Between 20 and 35 movies were used to quantify the effects of different treatments. To quantify the Cav1 cell-edge pool in suspended cells, cells were stained with the PM marker wheat germ agglutinin–Rhodamine at 0.01 mg/ml (WGA); using CellProfiler, nuclei were identified initially and the whole cell was delimited by the WGA staining. The average width of the PM, defined by WGA, was determined by measuring the number of pixels containing signal above background in 24 areas of the PM. This value was 3.16±0.19 pixels. Using this width (3 pixels) the outer border of the cell was automatically shrunk and the difference between the whole cell and the 'shrunk cell' was defined as the PM region. Cav1 signal in the cell and in the PM regions was measured and the signal in the PM was normalized to the cell signal in each object; this value was used to determine the amount of Cav1 at the cell edge (the region labeled by WGA). Cav1 linearity in Fig. 3A was determined blindly by measuring the total length of the linear pattern created by Cav1 spots in each cell. To quantify F-actin distribution in the cell, we segmented the cells stained with DAPI and phalloidin and set the cell center in the cell nucleus, from which 10 concentrically drawn areas were used to calculate the average intensity. To quantify stress fibers, cells were stained with DAPI and phalloidin and imaged with an Opera HCS System. An automated analysis routine was implemented using Definiens Developer (Definiens, München, Germany) to obtain quantitative values that describe actin stress fiber organization, which will be described elsewhere. In brief, a segmentation procedure delimits the cells and the 5 layers of pixels adjacent to the border are discarded from the analysis to avoid interference with cortical actin pools. Fibrillar actin structures were delimited using a segmentation routine and the area of these structures was measured. The ratio of segmented fibrillar actin area and the analyzed cellular area is calculated for every individual cell as a measurement of cellular stress fiber organization. For the analysis of Cav1 spot intensity values, we used Definies Developer. We first obtained an estimation of the image background intensity for each image by applying a histogram shape-based automatic threshold. Next, local maximums based on image contrast values were identified. These local maximum regions of interest (ROI) were considered if their intensity values lied above the background intensity value. Next, the centroid of each ROI defined as its highest intensity pixel was identified. From this pixel a circle of 5 pixels radius (Q5), corresponding to 49 pixels in the discrete image space, was defined. We discarded any overlapping Q5 circles to identify relatively isolated spots; these represented a small fraction of all objects. For each spot, the intensity value was calculated within the Q5 circle. At least 5000 spots were identified for each condition. With this intensity distribution, the range of spot intensity values in each quartile for the control sample was calculated and the proportion of spot intensity values in that range in the treated condition was calculated. The Cav1 spot intensity values were separated in four categories (q1, q2, q3, q4) defined by the four quartiles of the distribution of the control intensities. That is, q1 will contain vesicles with intensity levels between the minimum and the first quartile, q2 between quartile 2 and the median of the control data, and so on. Colocalization of GFP–mDia1 and Cav1 by TIRF-m was quantified using the Pearson's correlation coefficient, *r*. A circular ROI (0.45 µm diameter) was plotted in each green spot (GFP or GFP–mDia1) and *r* values above 0.7 were considered to indicate reliable colocalization.

Statistical analysis

Mean values were compared by two-tailed paired Student's *t*-test. *P*-values below 0.05 were considered statistically significant and were labeled with an asterisk. Data is represented as the mean ± s.e.m., unless otherwise indicated. Mann–Whitney non-parametric test was used to compare the complete distribution of vesicle intensities across conditions. To compare proportions, a proportions test based on a χ^2-test was used.

Electron microscopy

HeLa cells were processed for electron microscopy following standard procedures. Briefly, cells were fixed in 2% glutaraldehyde, 2% tannic acid in Hepes, and then post-fixed in 1% osmium tetroxide, 0.8% potassium ferrocyanide, followed by treatment with 2% uranyl acetate. The samples were dehydrated with acetone and embedded in Epon, sectioned, and stained. Ruthenium red (1 mg/ml) was added during fixation (without tannic acid) and osmification. To quantify the number of caveolae per sample, the total membrane length analyzed was estimated using ImageJ software. Morphologically defined single caveolae at the plasma membrane or caveolar domain containing rosettes (herein rosette-caveolae; with caveolae connected with the plasma membrane or separated from the plasma membrane) were scored. Caveolar domains above 100 nm in diameter where not scored. PM was categorized as straight (if a line of a minimum of 500 nm could be drawn over the PM without leaving the PM path) or contoured. Immunolabeling was performed following standard procedures. Briefly, HeLa cell monolayers were subjected to mild fixation in 4% paraformaldehyde containing 0.1% glutaraldehyde in PBS at 4℃ for 30 minutes, cryoprotected with glycerol and quickly frozen in liquid ethane. Freeze-substitution of vitrified specimens was performed in methanol containing 0.5% uranyl acetate. Samples were then infiltrated in Lowicryl HM20 Resin, polymerized, and ultrathin sections mounted on grids. Immunolabeling was performed with polyclonal anti-caveolin antibody diluted 1:20 in TBG buffer [30 mM Tris-HCl (pH 8.2), 150 mM NaCl, 0.1% BSA and 1% gelatine] and a secondary antibody conjugated to 10-nm-diameter gold particles. Gold particles within 0–50 nm of the cell edge were considered to mark an epitope at the PM. The signal was normalized to the gold signal intensity over the cell area analyzed. All analyses were performed with a JEOL 1230 transmission electron microscope operated at 100 kV.

Acknowledgements

We thank A. M. Pendergast, T. Koleske, J. Wehland, K. Rottner, S. Narumiya, R. Wedlich-Soldner and F. Sánchez-Madrid for valuable reagents. We thank S. Sánchez for excellent technical assistance, S. Calleja, I. Salanueva, C. Patiño, J. Bueno, I. Cotillo and the Centro Nacional de Investigaciones Cardiovasculares Microscopy Unit for technical assistance. We thank S. Bartlett and T. Pellinen for critical reading of the manuscript and R. Parton and A. G. Arroyo for helpful suggestions.

Funding

This work was supported by the Spanish Ministry of Economy and Competitiveness through the Ramón y Cajal Program to A.E.; a predoctoral fellowship from the Instituto de Salud Carlos III to O.M.; Ministry of Economy and Competitiveness grants SAF2008-02100, SAF2011-25047, RTICC RD06/0020/1033 and CSD 2009-00016 to M.A.d.P.; SAF2008-00451, SAF201122988 and RD06/0020/1001 to O.L.; Fondo de Investigaciones Sanitarias PS09/01028 to M.M. M.A.d.P. was funded by the European Heads of Research Councils, the European Science Foundation through a European Young Investigator award and by the EMBO Young Investigator Programme 2005-1211. The CNIC is supported by the MINECO and the Pro-CNIC Foundation.

Supplementary material available online at
http://jcs.biologists.org/lookup/suppl/doi:10.1242/jcs.090134/-/DC1

References

Aboulaich, N., Vainonen, J. P., Strålfors, P. and Vener, A. V. (2004). Vectorial proteomics reveal targeting, phosphorylation and specific fragmentation of polymerase I and transcript release factor (PTRF) at the surface of caveolae in human adipocytes. *Biochem. J.* **383**, 237-248.

Balasubramanian, N., Scott, D. W., Castle, J. D., Casanova, J. E. and Schwartz, M. A. (2007). Arf6 and microtubules in adhesion-dependent trafficking of lipid rafts. *Nat. Cell Biol.* **9**, 1381-1391.

Barilá, D. and Superti-Furga, G. (1998). An intramolecular SH3-domain interaction regulates c-Abl activity. *Nat. Genet.* **18**, 280-282.

Boucrot, E., Howes, M. T., Kirchhausen, T. and Parton, R. G. (2011). Redistribution of caveolae during mitosis. *J. Cell Sci.* **124**, 1965-1972.

Boyle, S. N., Michaud, G. A., Schweitzer, B., Predki, P. F. and Koleske, A. J. (2007). A critical role for cortactin phosphorylation by Abl-family kinases in PDGF-induced dorsal-wave formation. *Curr. Biol.* **17**, 445-451.

Bradley, W. D. and Koleske, A. J. (2009). Regulation of cell migration and morphogenesis by Abl-family kinases: emerging mechanisms and physiological contexts. *J. Cell Sci.* **122**, 3441-3454.

Bradley, W. D., Hernández, S. E., Settleman, J. and Koleske, A. J. (2006). Integrin signaling through Arg activates p190RhoGAP by promoting its binding to p120RasGAP and recruitment to the membrane. *Mol. Biol. Cell* **17**, 4827-4836.

Bundgaard, M., Hagman, P. and Crone, C. (1983). The three-dimensional organization of plasmalemmal vesicular profiles in the endothelium of rat heart capillaries. *Microvasc. Res.* **25**, 358-368.

Burton, E. A., Plattner, R. and Pendergast, A. M. (2003). Abl tyrosine kinases are required for infection by Shigella flexneri. *EMBO J.* **22**, 5471-5479.

Butler, B., Gao, C., Mersich, A. T. and Blystone, S. D. (2006). Purified integrin adhesion complexes exhibit actin-polymerization activity. *Curr. Biol.* **16**, 242-251.

Cai, C., Weisleder, N., Ko, J. K., Komazaki, S., Sunada, Y., Nishi, M., Takeshima, H. and Ma, J. (2009). Membrane repair defects in muscular dystrophy are linked to altered interaction between MG53, caveolin-3, and dysferlin. *J. Biol. Chem.* **284**, 15894-15902.

Cerezo, A., Guadamillas, M. C., Goetz, J. G., Sánchez-Perales, S., Klein, E., Assoian, R. K. and del Pozo, M. A. (2009). The absence of caveolin-1 increases

proliferation and anchorage-independent growth by a Rac-dependent, Erk-independent mechanism. *Mol. Cell. Biol.* **29**, 5046-5059.

Chan, M. W., Chaudary, F., Lee, W., Copeland, J. W. and McCulloch, C. A. (2010). Force-induced myofibroblast differentiation through collagen receptors is dependent on mammalian diaphanous (mDia). *J. Biol. Chem.* **285**, 9273-9281.

Chhabra, E. S. and Higgs, H. N. (2007). The many faces of actin: matching assembly factors with cellular structures. *Nat. Cell Biol.* **9**, 1110-1121.

Colbert, M. J., Raegen, A. N., Fradin, C. and Dalnoki-Veress, K. (2009). Adhesion and membrane tension of single vesicles and living cells using a micropipette-based technique. *Eur. Phys. J. E. Soft Matter* **30**, 117-121.

Colicelli, J. (2010). ABL tyrosine kinases: evolution of function, regulation, and specificity. *Sci. Signal.* **3**, re6.

Dai, Z. and Pendergast, A. M. (1995). Abi-2, a novel SH3-containing protein interacts with the c-Abl tyrosine kinase and modulates c-Abl transforming activity. *Genes Dev.* **9**, 2569-2582.

del Pozo, M. A., Alderson, N. B., Kiosses, W. B., Chiang, H. H., Anderson, R. G. and Schwartz, M. A. (2004). Integrins regulate Rac targeting by internalization of membrane domains. *Science* **303**, 839-842.

del Pozo, M. A., Balasubramanian, N., Alderson, N. B., Kiosses, W. B., Grande-García, A., Anderson, R. G. and Schwartz, M. A. (2005). Phospho-caveolin-1 mediates integrin-regulated membrane domain internalization. *Nat. Cell Biol.* **7**, 901-908.

Echarri, A., Lai, M. J., Robinson, M. R. and Pendergast, A. M. (2004). Abl interactor 1 (Abi-1) wave-binding and SNARE domains regulate its nucleocytoplasmic shuttling, lamellipodium localization, and wave-1 levels. *Mol. Cell. Biol.* **24**, 4979-4993.

Fujimoto, T., Miyawaki, A. and Mikoshiba, K. (1995). Inositol 1,4,5-trisphosphate receptor-like protein in plasmalemmal caveolae is linked to actin filaments. *J. Cell Sci.* **108**, 7-15.

Gaus, K., Le Lay, S., Balasubramanian, N. and Schwartz, M. A. (2006). Integrin-mediated adhesion regulates membrane order. *J. Cell Biol.* **174**, 725-734.

Goetz, J. G., Minguet, S., Navarro-Lérida, I., Lazcano, J. J., Samaniego, R., Calvo, E., Tello, M., Osteso-Ibáñez, T., Pellinen, T., Echarri, A. et al. (2011). Biomechanical remodeling of the microenvironment by stromal caveolin-1 favors tumor invasion and metastasis. *Cell* **146**, 148-163.

Goley, E. D. and Welch, M. D. (2006). The ARP2/3 complex: an actin nucleator comes of age. *Nat. Rev. Mol. Cell Biol.* **7**, 713-726.

Grande-García, A., Echarri, A., de Rooij, J., Alderson, N. B., Waterman-Storer, C. M., Valdivielso, J. M. and del Pozo, M. A. (2007). Caveolin-1 regulates cell polarization and directional migration through Src kinase and Rho GTPases. *J. Cell Biol.* **177**, 683-694.

Grevengoed, E. E., Fox, D. T., Gates, J. and Peifer, M. (2003). Balancing different types of actin polymerization at distinct sites: roles for Abelson kinase and Enabled. *J. Cell Biol.* **163**, 1267-1279.

Hansen, C. G. and Nichols, B. J. (2010). Exploring the caves: cavins, caveolins and caveolae. *Trends Cell Biol.* **20**, 177-186.

Hansen, C. G., Howard, G. and Nichols, B. J. (2011). Pacsin 2 is recruited to caveolae and functions in caveolar biogenesis. *J. Cell Sci.* **124**, 2777-2785.

Hayakawa, K., Tatsumi, H. and Sokabe, M. (2011). Actin filaments function as a tension sensor by tension-dependent binding of cofilin to the filament. *J. Cell Biol.* **195**, 721-727.

Hayer, A., Stoeber, M., Ritz, D., Engel, S., Meyer, H. H. and Helenius, A. (2010). Caveolin-1 is ubiquitinated and targeted to intralumenal vesicles in endolysosomes for degradation. *J. Cell Biol.* **191**, 615-629.

Hernández, S. E., Krishnaswami, M., Miller, A. L. and Koleske, A. J. (2004). How do Abl family kinases regulate cell shape and movement? *Trends Cell Biol.* **14**, 36-44.

Higashida, C., Miyoshi, T., Fujita, A., Oceguera-Yanez, F., Monypenny, J., Andou, Y., Narumiya, S. and Watanabe, N. (2004). Actin polymerization-driven molecular movement of mDia1 in living cells. *Science* **303**, 2007-2010.

Higgs, H. N. and Pollard, T. D. (2001). Regulation of actin filament network formation through ARP2/3 complex: activation by a diverse array of proteins. *Annu. Rev. Biochem.* **70**, 649-676.

Hill, M. M., Bastiani, M., Luetterforst, R., Kirkham, M., Kirkham, A., Nixon, S. J., Walser, P., Abankwa, D., Oorschot, V. M., Martin, S. et al. (2008). PTRF-Cavin, a conserved cytoplasmic protein required for caveola formation and function. *Cell* **132**, 113-124.

Innocenti, M., Gerboth, S., Rottner, K., Lai, F. P., Hertzog, M., Stradal, T. E., Frittoli, E., Didry, D., Polo, S., Disanza, A. et al. (2005). Abi1 regulates the activity of N-WASP and WAVE in distinct actin-based processes. *Nat. Cell Biol.* **7**, 969-976.

Ishizaki, T., Morishima, Y., Okamoto, M., Furuyashiki, T., Kato, T. and Narumiya, S. (2001). Coordination of microtubules and the actin cytoskeleton by the Rho effector mDia1. *Nat. Cell Biol.* **3**, 8-14.

Kang, Y. S., Ko, Y. G. and Seo, J. S. (2000). Caveolin internalization by heat shock or hyperosmotic shock. *Exp. Cell Res.* **255**, 221-228.

Kanzaki, M. and Pessin, J. E. (2002). Caveolin-associated filamentous actin (Cav-actin) defines a novel F-actin structure in adipocytes. *J. Biol. Chem.* **277**, 25867-25869.

Koleske, A. J., Baltimore, D. and Lisanti, M. P. (1995). Reduction of caveolin and caveolae in oncogenically transformed cells. *Proc. Natl. Acad. Sci. USA* **92**, 1381-1385.

Kozera, L., White, E. and Calaghan, S. (2009). Caveolae act as membrane reserves which limit mechanosensitive I(Cl,swell) channel activation during swelling in the rat ventricular myocyte. *PLoS ONE* **4**, e8312.

Le Lay, S., Hajduch, E., Lindsay, M. R., Le Lièpvre, X., Thiele, C., Ferré, P., Parton, R. G., Kurzchalia, T., Simons, K. and Dugail, I. (2006). Cholesterol-induced caveolin targeting to lipid droplets in adipocytes: a role for caveolar endocytosis. *Traffic* **7**, 549-561.

Leng, Y., Zhang, J., Badour, K., Arpaia, E., Freeman, S., Cheung, P., Siu, M. and Siminovitch, K. (2005). Abelson-interactor-1 promotes WAVE2 membrane translocation and Abelson-mediated tyrosine phosphorylation required for WAVE2 activation. *Proc. Natl. Acad. Sci. USA* **102**, 1098-1103.

Lewis, J. M., Baskaran, R., Taagepera, S., Schwartz, M. A. and Wang, J. Y. (1996). Integrin regulation of c-Abl tyrosine kinase activity and cytoplasmic-nuclear transport. *Proc. Natl. Acad. Sci. USA* **93**, 15174-15179.

Lommel, S., Benesch, S., Rottner, K., Franz, T., Wehland, J. and Kühn, R. (2001). Actin pedestal formation by enteropathogenic Escherichia coli and intracellular motility of Shigella flexneri are abolished in N-WASP-defective cells. *EMBO Rep.* **2**, 850-857.

Moren, B., Shah, C., Howes, M. T., Schieber, N. L., McMahon, H. T., Parton, R. G., Daumke, O. and Lundmark, R. (2012). EHD2 regulates caveolar dynamics via ATP-driven targeting and oligomerization. *Mol. Biol. Cell* **23**, 1316-1329.

Morone, N., Fujiwara, T., Murase, K., Kasai, R. S., Ike, H., Yuasa, S., Usukura, J. and Kusumi, A. (2006). Three-dimensional reconstruction of the membrane skeleton at the plasma membrane interface by electron tomography. *J. Cell Biol.* **174**, 851-862.

Mundy, D. I., Machleidt, T., Ying, Y. S., Anderson, R. G. and Bloom, G. S. (2002). Dual control of caveolar membrane traffic by microtubules and the actin cytoskeleton. *J. Cell Sci.* **115**, 4327-4339.

Muriel, O., Echarri, A., Hellriegel, C., Pavón, D. M., Beccari, L. and Del Pozo, M. A. (2011). Phosphorylated filamin A regulates actin-linked caveolae dynamics. *J. Cell Sci.* **124**, 2763-2776.

Nethe, M., Anthony, E. C., Fernandez-Borja, M., Dee, R., Geerts, D., Hensbergen, P. J., Deelder, A. M., Schmidt, G. and Hordijk, P. L. (2010). Focal-adhesion targeting links caveolin-1 to a Rac1-degradation pathway. *J. Cell Sci.* **123**, 1948-1958.

Palazzo, A. F., Cook, T. A., Alberts, A. S. and Gundersen, G. G. (2001). mDia mediates Rho-regulated formation and orientation of stable microtubules. *Nat. Cell Biol.* **3**, 723-729.

Parsons, J. T., Horwitz, A. R. and Schwartz, M. A. (2010). Cell adhesion: integrating cytoskeletal dynamics and cellular tension. *Nat. Rev. Mol. Cell Biol.* **11**, 633-643.

Parton, R. G. and Simons, K. (2007). The multiple faces of caveolae. *Nat. Rev. Mol. Cell Biol.* **8**, 185-194.

Parton, R. G., Joggerst, B. and Simons, K. (1994). Regulated internalization of caveolae. *J. Cell Biol.* **127**, 1199-1215.

Parton, R. G., Way, M., Zorzi, N. and Stang, E. (1997). Caveolin-3 associates with developing T-tubules during muscle differentiation. *J. Cell Biol.* **136**, 137-154.

Parton, R. G., Molero, J. C., Floetenmeyer, M., Green, K. M. and James, D. E. (2002). Characterization of a distinct plasma membrane macrodomain in differentiated adipocytes. *J. Biol. Chem.* **277**, 46769-46778.

Pelkmans, L. and Zerial, M. (2005). Kinase-regulated quantal assemblies and kiss-and-run recycling of caveolae. *Nature* **436**, 128-133.

Pelkmans, L., Kartenbeck, J. and Helenius, A. (2001). Caveolar endocytosis of simian virus 40 reveals a new two-step vesicular-transport pathway to the ER. *Nat. Cell Biol.* **3**, 473-483.

Pelkmans, L., Püntener, D. and Helenius, A. (2002). Local actin polymerization and dynamin recruitment in SV40-induced internalization of caveolae. *Science* **296**, 535-539.

Pelkmans, L., Bürli, T., Zerial, M. and Helenius, A. (2004). Caveolin-stabilized membrane domains as multifunctional transport and sorting devices in endocytic membrane traffic. *Cell* **118**, 767-780.

Peters, P. J., Mironov, A., Jr, Peretz, D., van Donselaar, E., Leclerc, E., Erpel, S., DeArmond, S. J., Burton, D. R., Williamson, R. A., Vey, M. et al. (2003). Trafficking of prion proteins through a caveolae-mediated endosomal pathway. *J. Cell Biol.* **162**, 703-717.

Plattner, R., Irvin, B. J., Guo, S., Blackburn, K., Kazlauskas, A., Abraham, R. T., York, J. D. and Pendergast, A. M. (2003). A new link between the c-Abl tyrosine kinase and phosphoinositide signalling through PLC-gamma1. *Nat. Cell Biol.* **5**, 309-319.

Pol, A., Luetterforst, R., Lindsay, M., Heino, S., Ikonen, E. and Parton, R. G. (2001). A caveolin dominant negative mutant associates with lipid bodies and induces intracellular cholesterol imbalance. *J. Cell Biol.* **152**, 1057-1070.

Reeves, P. M., Bommarius, B., Lebeis, S., McNulty, S., Christensen, J., Swimm, A., Chahroudi, A., Chavan, R., Feinberg, M. B., Veach, D. et al. (2005). Disabling poxvirus pathogenesis by inhibition of Abl-family tyrosine kinases. *Nat. Med.* **11**, 731-739.

Reginato, M. J., Mills, K. R., Paulus, J. K., Lynch, D. K., Sgroi, D. C., Debnath, J., Muthuswamy, S. K. and Brugge, J. S. (2003). Integrins and EGFR coordinately regulate the pro-apoptotic protein Bim to prevent anoikis. *Nat. Cell Biol.* **5**, 733-740.

Richter, T., Floetenmeyer, M., Ferguson, C., Galea, J., Goh, J., Lindsay, M. R., Morgan, G. P., Marsh, B. J. and Parton, R. G. (2008). High-resolution 3D quantitative analysis of caveolar ultrastructure and caveola-cytoskeleton interactions. *Traffic* **9**, 893-909.

Riedl, J., Crevenna, A. H., Kessenbrock, K., Yu, J. H., Neukirchen, D., Bista, M., Bradke, F., Jenne, D., Holak, T. A., Werb, Z. et al. (2008). Lifeact: a versatile marker to visualize F-actin. *Nat. Methods* **5**, 605-607.

Rizzo, V., Sung, A., Oh, P. and Schnitzer, J. E. (1998). Rapid mechanotransduction in situ at the luminal cell surface of vascular endothelium and its caveolae. *J. Biol. Chem.* **273**, 26323-26329.
Rothberg, K. G., Heuser, J. E., Donzell, W. C., Ying, Y. S., Glenney, J. R. and Anderson, R. G. (1992). Caveolin, a protein component of caveolae membrane coats. *Cell* **68**, 673-682.
Sanguinetti, A. R. and Mastick, C. C. (2003). c-Abl is required for oxidative stress-induced phosphorylation of caveolin-1 on tyrosine 14. *Cell. Signal.* **15**, 289-298.
Schwartz, M. A. (1997). Integrins, oncogenes, and anchorage independence. *J. Cell Biol.* **139**, 575-578.
Senju, Y., Itoh, Y., Takano, K., Hamada, S. and Suetsugu, S. (2011). Essential role of PACSIN2/syndapin-II in caveolae membrane sculpting. *J. Cell Sci.* **124**, 2032-2040.
Sharma, D. K., Brown, J. C., Choudhury, A., Peterson, T. E., Holicky, E., Marks, D. L., Simari, R., Parton, R. G. and Pagano, R. E. (2004). Selective stimulation of caveolar endocytosis by glycosphingolipids and cholesterol. *Mol. Biol. Cell* **15**, 3114-3122.
Sinha, B., Köster, D., Ruez, R., Gonnord, P., Bastiani, M., Abankwa, D., Stan, R. V., Butler-Browne, G., Vedie, B., Johannes, L. et al. (2011). Cells respond to mechanical stress by rapid disassembly of caveolae. *Cell* **144**, 402-413.
Smith-Pearson, P. S., Greuber, E. K., Yogalingam, G. and Pendergast, A. M. (2010). Abl kinases are required for invadopodia formation and chemokine-induced invasion. *J. Biol. Chem.* **285**, 40201-40211.
Stahlhut, M. and van Deurs, B. (2000). Identification of filamin as a novel ligand for caveolin-1: evidence for the organization of caveolin-1-associated membrane domains by the actin cytoskeleton. *Mol. Biol. Cell* **11**, 325-337.
Stoeber, M., Stoeck, I. K., Hanni, C., Bleck, C. K., Balistreri, G. and Helenius, A. (2012). Oligomers of the ATPase EHD2 confine caveolae to the plasma membrane through association with actin. *EMBO J.* **31**, 2350-2364.
Tagawa, A., Mezzacasa, A., Hayer, A., Longatti, A., Pelkmans, L. and Helenius, A. (2005). Assembly and trafficking of caveolar domains in the cell: caveolae as stable, cargo-triggered, vesicular transporters. *J. Cell Biol.* **170**, 769-779.
Tamura, K., Mizutani, T., Haga, H. and Kawabata, K. (2010). Nano-mechanical properties of living cells expressing constitutively active RhoA effectors. *Biochem. Biophys. Res. Commun.* **403**, 363-367.
Tanos, B. and Pendergast, A. M. (2006). Abl tyrosine kinase regulates endocytosis of the epidermal growth factor receptor. *J. Biol. Chem.* **281**, 32714-32723.
Thomsen, P., Roepstorff, K., Stahlhut, M. and van Deurs, B. (2002). Caveolae are highly immobile plasma membrane microdomains, which are not involved in constitutive endocytic trafficking. *Mol. Biol. Cell* **13**, 238-250.
Verma, P., Ostermeyer-Fay, A. G. and Brown, D. A. (2010). Caveolin-1 induces formation of membrane tubules that sense actomyosin tension and are inhibited by polymerase I and transcript release factor/cavin-1. *Mol. Biol. Cell* **21**, 2226-2240.
Vogel, V. and Sheetz, M. (2006). Local force and geometry sensing regulate cell functions. *Nat. Rev. Mol. Cell Biol.* **7**, 265-275.
Watanabe, N., Kato, T., Fujita, A., Ishizaki, T. and Narumiya, S. (1999). Cooperation between mDia1 and ROCK in Rho-induced actin reorganization. *Nat. Cell Biol.* **1**, 136-143.
Wickström, S. A., Lange, A., Hess, M. W., Polleux, J., Spatz, J. P., Krüger, M., Pfaller, K., Lambacher, A., Bloch, W., Mann, M. et al. (2010). Integrin-linked kinase controls microtubule dynamics required for plasma membrane targeting of caveolae. *Dev. Cell* **19**, 574-588.
Williams, T. M. and Lisanti, M. P. (2005). Caveolin-1 in oncogenic transformation, cancer, and metastasis. *Am. J. Physiol. Cell Physiol.* **288**, C494-C506.
Woodring, P. J., Litwack, E. D., O'Leary, D. D., Lucero, G. R., Wang, J. Y. and Hunter, T. (2002). Modulation of the F-actin cytoskeleton by c-Abl tyrosine kinase in cell spreading and neurite extension. *J. Cell Biol.* **156**, 879-892.
Woodring, P. J., Hunter, T. and Wang, J. Y. (2003). Regulation of F-actin-dependent processes by the Abl family of tyrosine kinases. *J. Cell Sci.* **116**, 2613-2626.
Yu, J., Bergaya, S., Murata, T., Alp, I. F., Bauer, M. P., Lin, M. I., Drab, M., Kurzchalia, T. V., Stan, R. V. and Sessa, W. C. (2006). Direct evidence for the role of caveolin-1 and caveolae in mechanotransduction and remodeling of blood vessels. *J. Clin. Invest.* **116**, 1284-1291.
Zhan, L., Rosenberg, A., Bergami, K. C., Yu, M., Xuan, Z., Jaffe, A. B., Allred, C. and Muthuswamy, S. K. (2008). Deregulation of scribble promotes mammary tumorigenesis and reveals a role for cell polarity in carcinoma. *Cell* **135**, 865-878.
Zhu, H., Lin, P., De, G., Choi, K. H., Takeshima, H., Weisleder, N. and Ma, J. (2011). Polymerase transcriptase release factor (PTRF) anchors MG53 protein to cell injury site for initiation of membrane repair. *J. Biol. Chem.* **286**, 12820-12824.